ANL-7755

ANL-7755

Argonne National Laboratory

CHEMICAL ENGINEERING DIVISION
FUEL CYCLE TECHNOLOGY QUARTERLY REPORT
July, August, September 1970

by

D. S. Webster, A. A. Jonke, G. J. Bernstein,
N. M. Levitz, R. D. Pierce,
M. J. Steindler, and R. C. Vogel

The facilities of Argonne National Laboratory are owned by the United States Government. Under the terms of a contract (W-31-109-Eng-38) between the U. S. Atomic Energy Commission, Argonne Universities Association and The University of Chicago, the University employs the staff and operates the Laboratory in accordance with policies and programs formulated, approved and reviewed by the Association.

MEMBERS OF ARGONNE UNIVERSITIES ASSOCIATION

The University of Arizona	Kansas State University	The Ohio State University
Carnegie-Mellon University	The University of Kansas	Ohio University
Case Western Reserve University	Loyola University	The Pennsylvania State University
The University of Chicago	Marquette University	Purdue University
University of Cincinnati	Michigan State University	Saint Louis University
Illinois Institute of Technology	The University of Michigan	Southern Illinois University
University of Illinois	University of Minnesota	The University of Texas at Austin
Indiana University	University of Missouri	Washington University
Iowa State University	Northwestern University	Wayne State University
The University of Iowa	University of Notre Dame	The University of Wisconsin

Printed in the United States of America
Available from
National Technical Information Service
U.S. Department of Commerce
Springfield, Virginia 22151
Price: Printed Copy $3.00; Microfiche $0.65

ANL-7755
Chemical Separations Processes
for Plutonium and Uranium

ARGONNE NATIONAL LABORATORY
9700 South Cass Avenue
Argonne, Illinois 60439

CHEMICAL ENGINEERING DIVISION
FUEL CYCLE TECHNOLOGY QUARTERLY REPORT

July, August, September 1970

by

D. S. Webster, A. A. Jonke, G. J. Bernstein,
N. M. Levitz, R. D. Pierce,
M. J. Steindler, and R. C. Vogel

October 1970

Previous report in this series: ANL-7735

TABLE OF CONTENTS

LIST OF FIGURES

LIST OF TABLES

CHEMICAL ENGINEERING DIVISION

FUEL CYCLE TECHNOLOGY QUARTERLY REPORT

JULY, AUGUST, SEPTEMBER 1970

ABSTRACT

Work has been done during the period July through September 1970 on fuel cycle technology projects in the following areas: (1) development of a head-end process for LMFBR fuels, consisting of removal of stainless steel cladding in a zinc bath and subsequent reduction of the fuel oxide to metal, (2) laboratory-scale and pilot-scale work to develop a fluid-bed process for the conversion of uranium nitrate and plutonium nitrate solutions to an oxide form suitable for the fabrication of fuel shapes for LMFBR fuel, (3) development of X-ray fluorescence spectrometry as an in-line analytical method for determining the Pu/U ratio of oxide fuels during fabrication, and (4) development of a centrifugal contactor of small diameter and large length-to-diameter ratio for the plutonium isolation steps in the solvent extraction of LMFBR fuels.

SUMMARY

I. LIQUID METAL DECLADDING OF REACTOR FUEL

Head-end processing of LMFBR fuel will include fuel-subassembly handling, cladding removal, iodine removal, and introduction of fuel into the acid dissolution unit for subsequent aqueous processing. A liquid metal decladding procedure under development at Argonne involves dissolving the stainless steel cladding from uranium-plutonium oxide fuel with molten zinc at 800°C, then chemically reducing the uranium-plutonium oxide to metal using magnesium-zinc-calcium or magnesium-copper-calcium alloys at 800°C.

Decladding Kinetics

Additional information has been obtained on the rates and mechanisms of attack of stainless steel by zinc at 800°C. The zinc solutions studied contained up to 26 wt % stainless steel, and some solutions also contained 5 to 12 wt % nickel. Type 304 stainless steel tubes (3/4-in. OD, 5/8-in. wall, 4-in. long) were immersed in a bulk solution for 1 to 30 min, and the depth of zinc penetration, the weight loss, and the concentration of nickel in the bulk solution were measured.

Kinetic data show that the rate of zinc penetration into stainless steel is determined, to a first approximation, by the nickel concentration in the bulk liquid phase. The experimental results also show that practical penetration and decladding rates can be obtained in zinc slurries containing up to 26 wt % stainless steel, the highest content studied. However, a mixture containing 26 wt % steel is a paste-like slurry that cannot be completely poured from its containing vessel and would be difficult to transport as a fluid.

Process Demonstration Experiments

Equipment is being assembled and tested for small-scale decladding experiments with 100-g quantities of highly irradiated oxide fuel. In these experiments, the stainless steel cladding will be dissolved in zinc by immersing fuel elements in a zinc melt. The fuel oxide, after removal from the decladding solution, will be reduced to metal in a liquid salt-metal system. Objectives of this work are to determine the behavior of plutonium and fission products and to demonstrate the general process concept.

Engineering-Scale Experiments

In one concept of the liquid-metal decladding of LMFBR fuel, fuel subassemblies that are contained in a refractory metal basket are immersed in liquid zinc. Stainless steel components of the subassemblies (the shroud, cladding, and end hardware) are removed by the zinc, and the $(U,Pu,FP)O_2$ drops into the basket, which is subsequently lifted out of the melt. The objective of initial experiments was to determine the composition of basket contents after the decladding step.

The basket used for tests simulating the decladding of UO_2 consisted of top and bottom plates, four support posts, and a perforated cylindrical wall that rested on the bottom plate and was aligned by the posts. The wall contained approximately 100 1/16-in. holes that allowed zinc to pass into and out of the basket. After dissolution of stainless steel, the basket was lifted out of the melt and the furnace. Before the zinc-stainless steel heel could freeze in the basket, the wall was slid upward and the UO_2 and metal heel were scraped into a tray.

During decladding of charges that included UO_2 fines, a significant fraction ($\sim$10%) of the fines was transported out of the basket and into the melt. To decrease the quantity of fines transported out of the basket, modification of the basket design would be necessary.

About 10% of the iron originally present in the simulated subassemblies was contained in the metal heel scraped from the basket. The quantity of zinc-steel heel roughly equalled the quantity of UO_2. Improved separation of steel from the fuel oxide would be expected by agitation of the basket contents.

Six experiments were performed to determine the extent of zinc splashing as a result of gas released when fuel elements rupture during decladding. In an experiment, one or two simulated fuel elements were used. Each fuel element contained about 25 cm^3 of argon at pressures of 7 to 60 atm. The bottom few inches of a fuel element was immersed in molten zinc, and the extent of splashing when rupture occurred was observed. Although some zinc splashed out of the decladding vessel, partial control of splashing was achieved in one experiment by means of heat shields which also served as splash shields. The incorporation of splash shields in the design of a decladding vessel is expected to prevent melt being splashed out of the vessel.

Behavior of Volatile Fission Products

The generation rates, behavior, and emission limits of active xenon, krypton, iodine, and tritium isotopes during head-end processing of LMFBR fuel were examined.

Xenon and krypton, which remain in gaseous form during irradiation and processing, would be the major constituents of a pyrochemical head-end off-gas.

Iodine is expected to be largely in elemental form in highly irradiated fuel, although some CsI and FeI_2 may be present. When iodine is released from a fuel element immersed in a zinc decladding melt, it reacts with the zinc to form ZnI_2. The ZnI_2 further reacts with KCl in the molten salt to form KI, which is retained in the salt (the salt is later stored as radioactive waste).

Only a small amount of gaseous tritium would be retained in fuel elements fed to the head-end step. Any tritium would probably accompany the xenon and krypton.

A conceptual pyrochemical head end provides for the liquid zinc decladding of fuel subassemblies and the reduction of fuel oxide to metal in the same closed furnace compartment. An advantage of this process is that the noble fission gases would be completely removed from the fuel in relatively small volumes of gas that could readily be stored in gas cylinders. Another advantage is that iodine would be completely separated from the fuel material during decladding and would be converted to a salt for ultimate storage as an active waste.

Laboratory-scale experiments simulating the release of iodine fission gas during decladding showed that reaction of iodine with molten zinc is extremely rapid and that decontamination factors of at least 10^5-10^6 are readily achieved.

II. CONTINUOUS CONVERSION OF U/Pu NITRATES TO OXIDES

A fluidized-bed process is under development for the conversion of uranium nitrate and plutonium nitrate to an oxide form suitable for the fabrication of fuel shapes for LMFBR fuel. A laboratory program in progress includes (1) study of the stability of the nitrate solutions and (2) denitration tests to determine the phases present in the final oxide product. A fluidized-bed pilot plant for the continuous denitration of uranium-plutonium solutions has been constructed.

Laboratory work showed the change in valence distribution of plutonium (VI) and (IV) ions in nitrate solution to be a zero-order reaction with respect to Pu(VI) for a 50-day period. After 50 days, the rate of decrease of Pu(VI) ions appeared to increase. The rate of valence change in the range 0.3 to 1.35M plutonium was independent of the initial plutonium concentration. No trivalent or pentavalent spectra were observed in the spectrophotometric examination of a 3M HNO_3 solution containing 1.35M plutonium.

X-ray diffraction patterns of PuO_2 prepared at 300°C by dropwise denitration of two solutions were compared. One solution contained 65% Pu(VI)-35% Pu(IV) nitrate and the other only Pu(IV). The PuO_2 prepared from the solution containing only Pu(IV) showed a more crystalline structure, but no other difference in the patterns was observed.

The pilot-scale fluid-bed system was checked out in a series of six denitration runs with uranyl nitrate. All runs were made at a denitration temperature of 300°C. Feed solutions contained 1-2.4M uranium and 0.2 to 1.0N excess acid. Feed rates ranged from 50 ml/min of 1M uranyl nitrate to 100 ml/min of 2.4M uranyl nitrate; these feed rates are equivalent to 22 and 105 lb $UO_3/(hr)(ft^2$ reactor cross section); the upper value slightly exceeds the design goal of 100 lb/(hr)(ft^2). Inlet fluidizing-air velocities were 1 to 1.5 ft/sec. Flow ratios of feed nozzle air (in scfm) to liquid (in cc/min) were in the range 330 to 640. Runs continued for as long as 14 hr.

Particle size effects were observed in this series of exploratory runs, but conclusions are considered tentative because of the relatively short durations of the experiments. Also, it may not be

possible to extrapolate these results to uranium-plutonium systems. Observed effects included the following: (1) slight overall growth of bed particles during the run was indicated by sieve analyses of the UO_3 product collected at half-hour intervals together with calculations of average particle size. (2) fines (-200 mesh) were produced in increasing quantity as the feed rate was increased; the bulk of the fines were collected on the sintered metal filters, which are mounted directly above the bed; fines production corresponded to about 5% of the total UO_3 produced in a run. (3) some coarse (+8 mesh) material formed, corresponding to about 5 to 10% of the UO_3 produced.

Product removal was effected by continuous overflow of bed material from a sidearm takeoff line, supplemented (in the final experiment reported) by intermittent withdrawal at the bottom of the column. Product removal at two locations allowed a fairly uniform bed inventory to be maintained. Sieve analyses showed the two product streams to have similar particle size distributions, indicating that good mixing was being achieved in the bed.

The current program has provided insight into the characteristics of denitration pilot plant operation and has shown that the equipment and instrumentation were functioning properly. Modifications of the equipment for work with uranium-plutonium systems are being planned.

III. IN-LINE ANALYSIS IN FUEL FABRICATION

The development of in-line nondestructive methods for analysis of critical fuel properties is necessary to lower the fuel fabrication costs for the large number of fuel subassemblies expected to be processed in the LMFBR program. The specifications of fuel properties (and the associated precisions) for the Fast Fuel Test Facility (FFTF) project have been selected as the starting criteria for evaluating methods of analysis.

X-ray fluorescence spectrometry is being evaluated as a direct method of measuring the uranium and plutonium content of oxide fuel in pellet or powder form. It has been demonstrated, utilizing powdered ThO_2-UO_2 as a stand-in for UO_2-PuO_2, that the method is promising for performing one analysis per minute.

IV. ADAPTATION OF CENTRIFUGAL CONTACTORS IN LMFBR FUEL PROCESSING

A centrifugal contactor of small diameter and large length-to-diameter ratio is being studied to extend centrifugal contactor design to a configuration suitable for the plutonium isolation steps in the solvent extraction of LMFBR fuels. The basic contactor is patterned after units in use at Savannah River.

A stainless steel unit is being built that has a 4 3/4-in. ID stator and a 4-in. ID by 0.1-in. wall rotor with a 12-in. high settling zone. This unit is designed to operate at speeds up to about 3600 rpm and is expected to have a capacity of about 12 gpm.

The basic Savannah River (SR) design has been modified in the

ANL stainless steel unit so that it can also be operated as an annular mixer. When the ANL contactor is operated as an annular mixer, the paddle and mixing chamber are absent and the solvent and aqueous streams enter the annular space between the wall of the stator (or casing) and the rotor. Mixing occurs by skin friction as the phases flow down through the annulus. The mixture next enters an orifice in the bottom of the hollow rotor (or bowl), and the phases are separated as they move upward in the rotor. Discharge of the phases at the top of the rotor is the same as in the SR design.

While the stainless steel unit is being fabricated, a simplified annular type of contactor fabricated of plastic is being used for preliminary testing. Tests with water only showed that throughputs of $\sim$10 gpm can be achieved at rotor speeds up to about 1650 rpm. Power input to liquid in the annulus has also been measured by means of a dynamometer. Results indicate that intensive mixing can be achieved with a smooth-walled rotor and stator.

I. LIQUID METAL DECLADDING OF REACTOR FUELS

(R. D. Pierce)

Liquid-metal decladding processes under development at Argonne appear to provide relatively simple and inexpensive techniques for solving formidable head-end processing problems[1] related to the high burnups, short cooling times, residual sodium, and high plutonium content of irradiated LMFBR fuels.

Early LMFBR fuel elements will consist of mixed uranium and plutonium oxides jacketed in stainless steel tubes. These fuels may be irradiated to burnups up to 100,000 MWd/ton at specific powers as high as 175 kW/kg and may be allowed to decay for only 30 days. The localized heat emission of LMFBR fuels is very high, creating heat-dissipation problems during handling and processing operations.

High concentrations of radioactive iodine (especially ^{131}I), xenon, and krypton in spent LMFBR fuel will present serious problems in handling and disposing of the waste-gas effluent from reprocessing operations. To avoid excessive emissions of ^{131}I to the environment, head-end operations must be performed in a sealed cell and fission gas must be efficiently removed from the fuel material prior to the nitric acid dissolution step of aqueous fuel processing.

If sodium is present in failed fuel elements, it too would present cleaning and fuel-dissolution problems since sodium can react explosively with nitric acid. In addition, the high plutonium content of LMFBR fuel presents severe criticality problems.

In liquid-metal decladding, cladding is removed by immersing a discharged fuel subassembly (probably after cropping the bottom) in a pool of molten zinc having molten salt cover layer. The zinc dissolves the stainless steel components (both the subassembly supporting members and the cladding) but does not react with the fuel oxides. This procedure avoids the requirement, in a shear-leach process, that the following operations be performed: mechanical disassembly, handling of individual fuel elements, and shearing of fuel hardware. Other advantages of liquid-metal decladding include (1) efficient removal of iodine and other volatile fission products, (2) relative ease of dissipation of fission-product heat, (3) elimination of the requirement for separate sodium-removal steps, (4) discharge of all process waste streams (except Xe and Kr) as solids having good heat transfer properties, (5) collection of xenon and krypton in an inert cover gas mixture (containing ~50% Xe plus Kr) that can be stored in gas cylinders, (6) absence of effective neutron-moderating elements, and (7) process simplicity and flexibility.

The principal disadvantages of liquid-metal decladding are the lack of industrial experience in the use of refractory metals and graphite as materials of construction, and the large quantities of reagent zinc discharged as waste. Refractory metals and graphite are compatible with

---

[1] C. D. Watson et al., "Proceedings of the 16th Conference on Remote Systems Technology," pp. 19-38, Amer. Nucl. Soc. (1969).

liquid zinc and molten salts. Equipment fabricated of these materials have long lives, but their cost is a significant portion of the processing cost. For each ton of fuel processed, about 15 ft^3 of zinc is discharged to waste. Solid zinc is an ideal waste form, and the reagent and waste-disposal costs are not large. An alternative to storage is recovery of the zinc by a zinc-vaporization process.

A. ENGINEERING DEVELOPMENT--DECLADDING KINETICS

(I. O. Winsch, T. R. Johnson, J. J. Stockbar, T. F. Cannon, R. W. Clark)

Removal of stainless steel from LMFBR fuel elements is being investigated as a head-end process to prepare discharged fast reactor fuels for introduction into fuel-recovery plants. Additional information has been obtained on the rate and mechanism of attack of stainless steel by zinc at 800°C. Earlier data (ANL-7735, pp. 14-15) had shown that liquid zinc rapidly penetrates stainless steels at 800°C, even when the bulk solutions are saturated with iron and chromium. Metallographic examinations reported earlier (ANL-7735, p. 15) indicated that the mechanism of attack is the leaching of nickel from the austenitic phase and the freeing of grains of iron-chromium alloy, which then are carried by zinc into the bulk solution.

In the experiments completed during this period, stainless steel dissolution rates were determined from the depths of zinc penetration into solid stainless steel samples immersed in Zn-Fe-Ni-Cr mixtures for known periods of time. The effects on the rates and mechanisms of liquid-metal decladding of (1) stainless steel and nickel concentrations in the melt and (2) agitator speed were studied.

1. Experimental Conditions

Two experiments (ZDS-12 and -13) were conducted to determine the relative rates of dissolution and penetration of stainless steel by zinc containing known concentrations of stainless steel and nickel. Previously unreported data for two earlier experiments, ZDS-5 and -6, are also included here.

The test procedure was to immerse a weighed sample of Type 304 stainless steel tube (3/4-in. OD, 5/8-in. ID, 4 in. long) for a specified time in ~10 kg of Zn-Fe-Cr-Ni melt[1a] held at 800°C in a 5 1/2-in.-ID tungsten crucible. The tube was immersed vertically, and the melt stirred with an agitator, 2 in. in dia and 0.53 in. high and having two blades pitched at a 45° angle. The agitator speed was varied from 0 to 500 rpm, but in most tests it was 100 rpm. After a tube was exposed for 1 to 30 min, it was removed from the zinc solution. The concentrations of iron, chromium, and nickel in the melt were not changed significantly by the dissolution of metal from a single sample. After tests at one melt composition were completed, additional stainless steel or nickel was added to

[1a] In two runs (ZDS-5 and -6), the melt contained 1% sodium. However, earlier work showed that this concentration of sodium has no effect on the decladding rate.

the melt, and stainless steel dissolution rates were measured in a melt having the new melt composition.

Some of the tubes that had been immersed were placed in a vacuum retort to remove adhering zinc, then weighed. The difference between the tube weight before immersion and the tube weight after retorting was the weight loss due to dissolution in zinc.

All of the tubes were sectioned, polished and etched. The thicknesses of the inner and outer reaction zones and of the unaffected steel were measured. The difference between the original thickness and of the tube wall thickness of unaffected steel after immersion was the depth of penetration of zinc into the stainless steel.

The composition of the liquid metal phase was determined by analyses for iron, chromium, and nickel or, in cases where samples were not obtained, the composition was calculated. This calculation was based on the assumptions that all of the nickel added was in the liquid phase, that the cosolubilities of iron and chromium in zinc at 800°C are 5.8 wt % and 1.0 wt %, respectively, and that the solid phase in equilibrium with the saturated zinc solution contains 45 wt % zinc. This composition of the solid phase is based on the published iron-zinc phase diagram.[2] The actual cosolubilities in the quaternary system have not been studied in detail, but the values of iron and chromium given above are averages of values found in our dissolution studies. In most cases, the calculated liquid compositions agreed well with the compositions determined by analysis of filtered samples. However, the analysis of a filtered sample taken at the end of ZDS-13 was approximately 3 wt % Fe, 0.6 wt % Cr and 8.5 wt % Ni compared with the calculated values of 5.8 wt % Fe, 1.0 wt % Cr, and 12.8 wt % Ni. This analysis is being checked.

2. Results and Discussion

This work indicates that the rate at which zinc penetrates into Type 304 stainless steel is primarily related to the nickel content of the liquid zinc phase. In run ZDS-12, depths of zinc penetration were determined for test pieces exposed to melts containing 15 to 26 wt % stainless steel and with agitation speeds of 0 and 500 rpm (see Table 1). With 15 to 19 wt % stainless steel in the melt, the nickel concentration in the solution was 1.42 to 1.97 wt % and the zinc penetration depth was 0.44 to 0.46 mm for a 5-min immersion time. With 20 to 26 wt % stainless steel in the melt, the melt contained 2.14 to 3.22 wt % nickel, and the penetration depth in 5 min was 0.41 to 0.42 mm. The agitator speed had no appreciable effect on the penetration depth.

The penetration of Type 304 stainless steel by zinc as measured in these experiments is shown in Fig. 1. In this graph, total compositions represent the total amounts of stainless steel and nickel added to the zinc and liquid compositions represent values calculated as described above. The data show that penetration of the stainless steel was rapid

---

[2] M. Hansen and K. Anderko, Constitution of Binary Alloys, McGraw-Hill, New York, 1958, p. 738.

Table 1

Zinc Penetration of Stainless Steel Tubes

Immersion Time: 5 min
Run: ZDS-12

Nominal Stainless Steel Content (wt %)	Nominal Stainless Steel Content (kg)	Nickel in Solution (wt %)	Zinc Penetration Depth[a] (mm)
15	1.765	1.42	0.46
16	1.922	[1.54][b]	0.45
17	2.050	[1.69][b]	0.44
18	2.206	1.82	0.46
19	2.354	[1.97][b]	0.44
20	2.504	2.14	0.42
22	2.851	2.35	0.41
24	3.258	2.81	0.42
26	3.595	3.22	0.42

[a] Average of results at 0- and 500-rpm agitator speeds.

[b] Calculated as described in text.

Figure 1

Penetration of Type 304 Stainless Steel by Zinc at 800°C

Agitator Speed: 100 rpm for ZDS 5, 6 and 13
0 and 500 rpm for ZDS 12

The slopes of the lines indicate steady-state penetration rates.
The compositions of the liquid for Curves A, B, C, D, and E are as follows:

A: Fe <1%; Cr <0.2; Ni <0.1
B: Fe, 5.2%; Cr, 1.0; Ni, 0.6
C: Fe, 5.8%; Cr, 1.0; Ni, 1.4
D: Fe, 5.8%, Cr, 1.0; Ni, 5.5
E: Fe, 5.8%; Cr, 1.0; Ni, 12.8

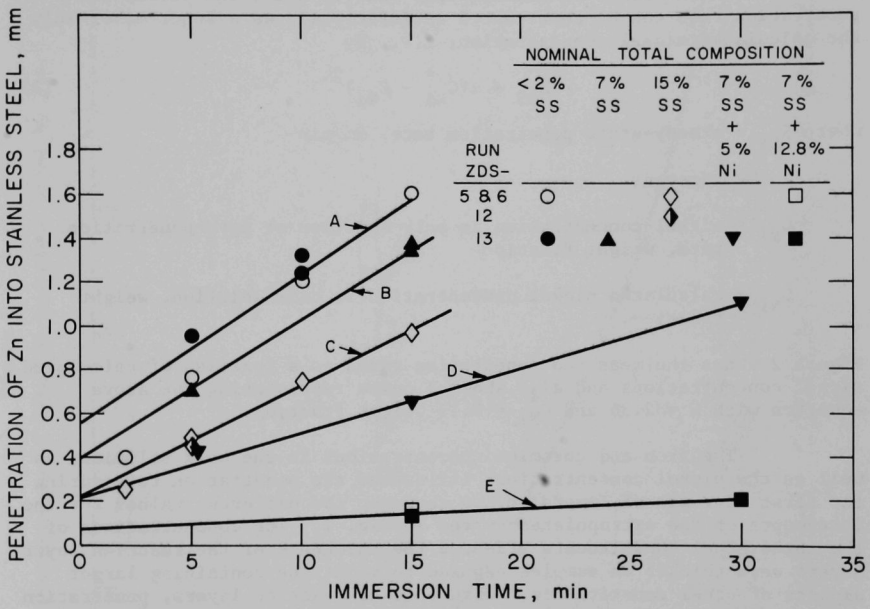

during the first 5 min of immersion, as indicated by the positive intercepts when the curves in Fig. 1 were extrapolated. After about 5 min of immersion time, the penetration rate decreased and the thickness of the reaction layer appeared to reach an equilibrium thickness, indicating that the rate of dissolution or removal of solids from the reaction layer and the rate of penetration were equal. The reaction layer had little strength at 800°C. It is believed that once the zinc has penetrated the steel cladding completely, the remaining cladding would crumble and for all practical purposes the fuel would be declad. It is believed that the penetration data are the most pertinent to the decladding studies.

On the basis of measurements made to date, the steady-state penetration rate can be represented satisfactorily as a function of only the calculated nickel concentration, *i.e.*, by

$$R_{SS} = \alpha(C_{Ni}^{*} - C_{Ni})^{2} \qquad (1)$$

where R_{SS} = steady-state penetration rate, mm/min

α = constant

C_{Ni}^{*} = nickel concentration in bulk solution at zero penetration rate, weight fraction

C_{Ni} = calculated nickel concentration in bulk solution, weight fraction.

Figure 2 shows the measured penetration rates as a function of calculated nickel concentrations and also shows a curve representing the above equation with α = 2.36 and C_{Ni}^{*} = 0.17 weight fraction.

The iron and chromium concentrations in the bulk solution, as well as the nickel concentration, influenced the penetration rate during the first five min of immersion, as shown by the different values for the intercepts of the extrapolated curves in Fig. 1. The concentrations of the three steel constituents affected the thickness of the reaction layer. Layers were thicker on samples exposed to solutions containing larger amounts of steel constituents. With thicker reaction layers, penetration rates were lower. Upon exposure of test pieces to solutions saturated with iron and chromium containing 5 to 13 wt % Ni, the samples grew in size and lost little if any weight, although the penetration rate was significant and could be predicted by Eq. 1.

At present, not enough measurements have been made to allow quantitative conclusions relating reaction layer thickness and weight loss to agitation rate and solution compositions. However, in melts not saturated with iron and chromium, the weight loss of samples was observed to be linear with exposure time and to depend on the concentrations of iron, chromium, and nickel in the melt and on the agitation rate.

In experiment ZDS-12, the limit to which the zinc solution could be loaded with stainless steel at 800°C was investigated, as well as the penetration rate. The highest stainless steel content obtained was 26 wt %. It was found that only 25% of this paste-like zinc-stainless steel

Figure 2

Penetration Rate of Type 304 Stainless Steel by Zinc

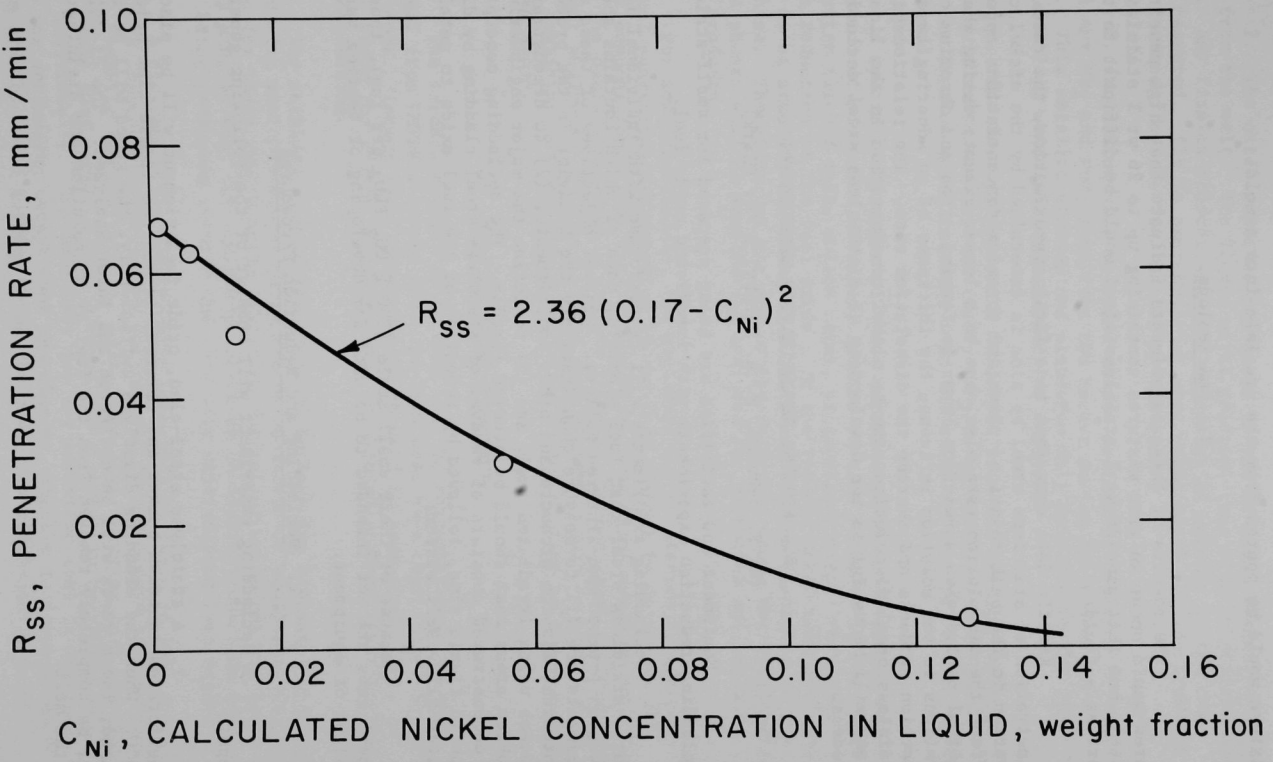

mixture would be poured from the crucible into a mold.

3. Conclusions

The results of these experiments indicate that high penetration rates would occur in zinc mixtures containing up to 26 wt % stainless steel, but that zinc-26 wt % stainless steel would be difficult to transport as a fluid.

Kinetic data show that to a first approximation, the rate of penetration of stainless steel by zinc is determined by the nickel concentration in the bulk solution. Iron and chromium concentrations appear to affect the dissolution rate also, but to a lesser extent; during the initial period when a reaction layer is forming, iron and chromium concentrations in the solution influence the thickness of an adhering layer of reaction products and thereby the dissolution rate. The relationship of stainless steel dissolution rate to nickel concentration in the liquid phase will be useful in the development of a stainless steel decladding process.

B. PROCESS DEMONSTRATION EXPERIMENTS

(T. R. Johnson, W. A. Murphy, R. W. Clark)

Equipment and facilities are being prepared for small-scale decladding-reduction experiments with irradiated oxide fuel.

Decladding experiments will be performed with individual irradiated stainless steel-clad fuel elements, each of which contains about 100 g of pressed-and-sintered pellets. General objectives of these experiments are (1) to measure quantitatively the behavior in the process of plutonium, fission products and other constituents, (2) to demonstrate the process using irradiated fuel, and (3) to define the major engineering problem areas that should be studied further. The decladding concept to be demonstrated consists of removal of stainless steel cladding by dissolution in liquid zinc, followed by reduction of the fuel oxide to metal in a molten alloy-salt system.

Because of their small scale (100 g UO_2-PuO_2 per run), these experiments are not intended to be used for developing or testing various designs of equipment.

1. Decladding and Reduction Procedures

A decladding experiment will consist of the following general steps:

1. A stainless steel-clad, oxide fuel element will be placed in a perforated tantalum basket and immersed in stirred liquid zinc held at 800°C. When the cladding dissolves sufficiently, the gases will be released; these gases will be collected and later analyzed. The cladding will be completely removed from the fuel by dissolution and disintegration in the melt.

2. The oxide pellets, contained in the tantalum basket, will be removed from the melt. The liquid metal solution then will be stirred and sampled. Any fission product activity appearing as solutes in the melt will be measured. (It is expected that some noble metal fission products will be leached from the fuel pellet by the zinc.)

3. Magnesium will be added to the decladding solution to reduce to metal any UO_2 and PuO_2 lost from the basket during the dissolution process. This metallic uranium and plutonium will dissolve in the zinc-magnesium alloy, which will be sampled for analysis.

4. The fuel pellets will be dumped from the tantalum basket into a liquid salt-metal system ($CaCl_2$-CaF_2/Cu-Mg-Ca) for reduction to metal. The fission gases released from the oxide matrix will be collected and analyzed.

A specific objective of these experiments is to determine the distribution of plutonium, uranium, and the fission products in the three-phase system (liquid salt, molten metal, precipitated metal) resulting from the reduction of the fuel oxide. In the various metal-salt reduction systems to be studied, plutonium is soluble and uranium insoluble in the metal phase. Therefore, at the end of the reduction step, the final metal and salt phases will be sampled and analyzed for plutonium and certain fission products.

For some experiments, the procedure may be altered to include mechanical puncturing and sampling of the fuel element to determine the chemical composition of the fuel. Mechanical puncturing would be done outside the decladding vessel, and the released fission gases trapped for subsequent analysis. Sections of the fuel elements would be examined, and the remaining portions would be declad in molten zinc by the procedure described above.

2. Materials and Equipment

The irradiated fuel to be used will be representative of the spent fuel from LMFBR's except that the fuel will have been cooled for a year or more. Intact fuel elements will be used in some experiments in order to study the effect of gas release on fission product distribution during decladding.

The shielded cave of the Chemical Engineering Division, which is equipped with manipulators allowing remote operation of equipment, has been prepared for these experiments. Existing decladding equipment has been modified and, to test the equipment, practice decladding-reduction runs are now being performed outside the cave with unirradiated fuel oxide.

A diagram of the experimental apparatus is shown in Fig. 3. Not shown are a thermocouple well that is immersed in the liquid zinc and a port for removing samples from the melt. The fuel-charging port has two sliding seals that permit a fuel element and a basket to be raised and lowered individually. The equipment for the reduction runs is the same as that for decladding except that the alumina crucible is removed and a tantalum crucible with baffles holds the reduction metal-salt system.

Figure 3

Experimental Set-Up for Decladding Runs

with Irradiated Fuel Elements

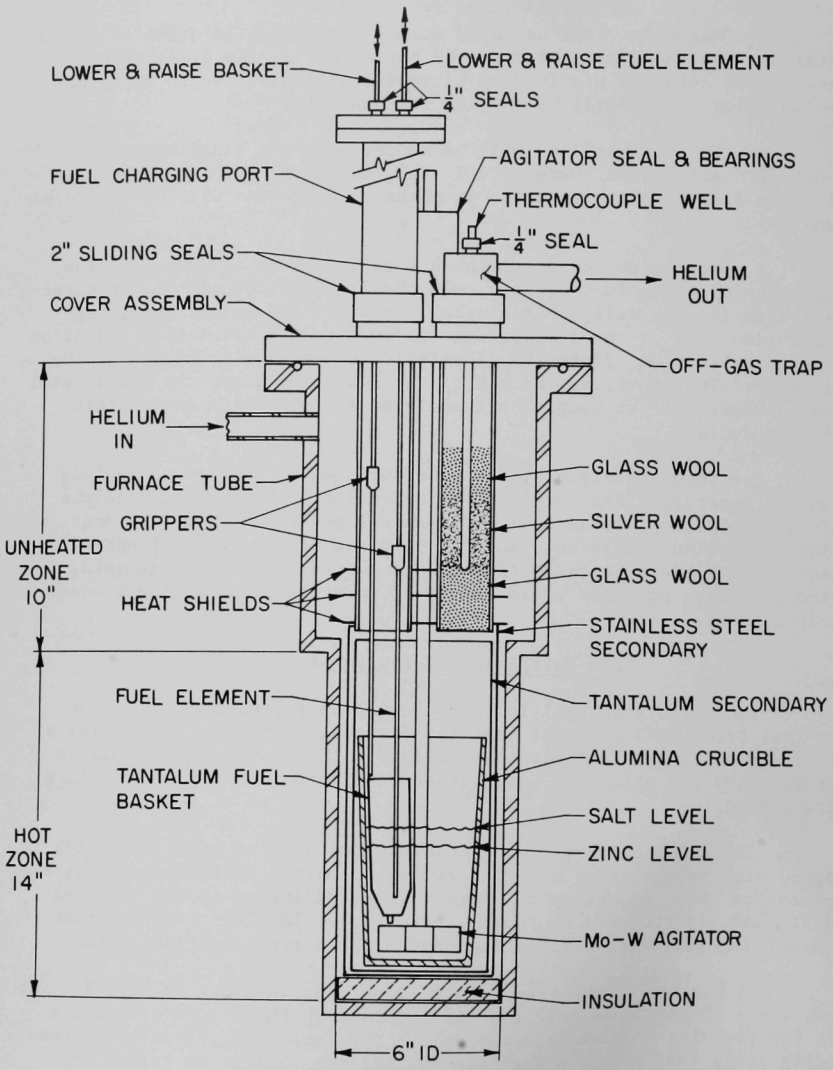

Oxide is charged to the tantalum crucible by immersing a loaded tantalum basket in the reduction alloy. (Before immersion, the open end of the basket is closed by a fusible magnesium plug.)

During an experiment, helium is circulated continuously through the furnace tube and a gas manifold. Gas from the manifold enters the furnace tube above the heat shields and leaves through the off-gas trap. This trap is packed with glass wool to remove zinc dust and other particulates and with silver wool to remove iodine. The exit gas passes over heated CuO to oxidize tritium and then through a Molecular Sieve bed cooled with liquid nitrogen in order to remove tritium oxide, xenon, krypton, and any other condensable gas. The helium is recompressed by a diaphragm pump and recirculated to the furnace tube. At the end of an experiment, the adsorbed gases are released by heating the Molecular Sieve beds. The quantity of adsorbed gases will be determined by a pressure measurement, and the composition of the gases will be determined.

C. ENGINEERING-SCALE EXPERIMENTS

(I. O. Winsch, T. F. Cannon, J. J. Stockbar)

1. Basket-Draining Experiments

In one concept of liquid-metal decladding of LMFBR fuel (ANL-7735, pp. 33-43), three fuel assemblies are contained in a basket during decladding in liquid zinc. After the stainless steel components of the subassembly (the shroud, cladding, and end hardware) are dissolved in the zinc, the basket (which contains UO_2-PuO_2) is lifted out of the zinc melt.

Several experiments have been performed to evaluate basket design and decladding techniques on the basis of the composition of the fuel oxide-metal heel in the drained basket. The basket initially used in these experiments consisted of a Mo-30 wt % W frame enclosed by a 70-mesh tungsten screen that allowed zinc to pass into and out of the basket. The screen proved too fragile for the operations performed and was replaced in the following three experiments with an 0.030-in.-wall tantalum cylinder containing approximately 100 1/16-in. holes (Fig. 4). The tantalum cylinder was 6 in. high; the holes were spaced at 1-in. intervals on the circumference and at 1/2-in. intervals up the lower 3 1/2 in. of the wall.

At the beginning of an experiment, the basket was charged with a stainless steel tube (4-in. OD, 1/8-in. wall, and 5-in. height) and UO_2 pellets or crushed pellets of a selected particle-size distribution (Table 2). (At present, the particle-size distribution for declad, irradiated LMFBR fuel is not known.) The melt (contained in a tungsten vessel) consisted of 65 kg of zinc covered with 3 kg of $MgCl_2$-30 mol % NaCl-20 mol % KCl. The basket and contents were immersed in zinc at 800°C, and the contents of the vessel were agitated at 300 rpm with a 3 3/4-in. slant-blade paddle. After a 2.5-hr exposure, the basket was removed from the melt. Before the basket cooled, the tantalum wall was slid upward, and the contents were scraped from the base of the basket into a stainless steel tray. The composition of the zinc-steel-UO_2 residue in the basket was determined by dissolving the material scraped from the basket in an

Figure 4

Experimental Decladding Basket (5 3/4 in. dia by 10 3/4 in. high) at the End of a Decladding Experiment

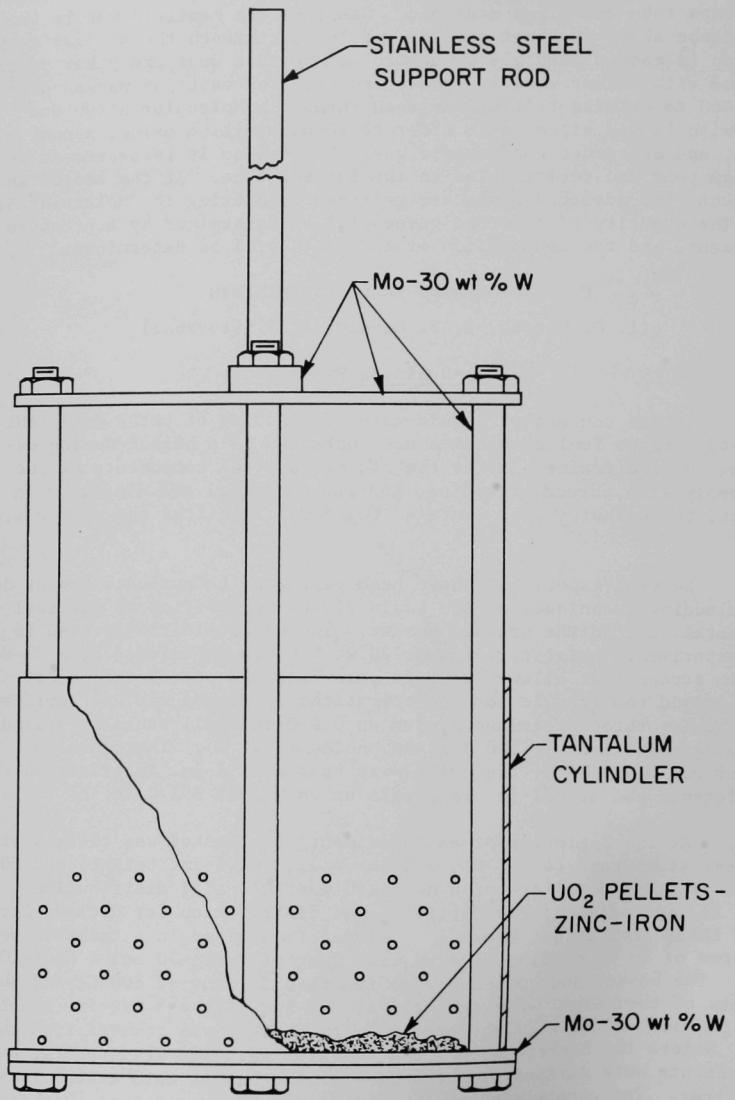

Table 2

Basket Draining Experiments

Melt: 65 kg of zinc, 3 kg of $MgCl_2$-30 mol % NaCl-20 mol % KCl

	Basket Charge			Retained in Basket			
	Uranium Oxide						
Run	Pellets[a] (kg)	Fines (kg)	Stainless Steel (kg)	Uranium (% of charge)	Iron (% of charge)	Zinc (kg)	Salt (kg)
SD-3	0.50	0	0.95	100	11	0.46	0.03
SD-4	0.25	0.11[b]	0.96	97.5	16.3	0.84	0.07
SD-5	0	0.20[c]	0.96	86.4	6.2	0.49	0.09

[a] 0.21-in. dia by 0.25-in. length.

[b]
-14 +25 mesh	0.05 kg
-25 +45 mesh	0.035 kg
-45 +80 mesh	0.025 kg

[c]
+14 mesh	0.10 kg
-80 +170 mesh	0.05 kg
-170 +325 mesh	0.05 kg

acid solution, acid-cleaning the basket to remove unscraped material, and analyzing the combined solutions. The results for the runs in which the tantalum cylinder was employed are presented in Table 2.

For two runs, in which a portion of the UO_2 charge was present as crushed pellets, a significant loss of oxide fines (~10%) from the basket was observed. The loss was greater when the oxide charge consisted entirely of fines. If the basket concept is to be applied to decladding fuel that contains an appreciable fraction of oxide fines, modification of the basket design may be necessary.

Any waste zinc-steel that is to be discarded must have a low plutonium content. If this decladding technique is adopted, some provision will be made to remove any UO_2 fines (perhaps by filtration of the melt) prior to discard.

Another objective of the decladding process is to achieve maximum separation of the fuel oxide from the stainless steel. In the three basket-draining experiments, about 10% of the iron originally in the simulated subassemblies was contained in the zinc-stainless steel heel. The quantity of heel roughly equalled the quantity of UO_2. Improved separation of steel from the fuel oxide may be achieved by sloshing or other agitation of the basket contents.

2. Gas-Release Experiments

Experiments have been performed simulating the release of high-pressure gas inside the shroud of a cropped fuel subassembly upon rupture of the cladding of a fuel element immersed in a zinc melt. About 5.7 moles of xenon and krypton is estimated to be contained in each core fuel subassembly (containing 217 fuel elements) of the reference Atomics International LMFBR fuel at a 6.7% burnup and 30-day cooling. The plenum of each fuel element is estimated to contain up to 0.026 mole of krypton and xenon, and if the fuel element temperature is 600°C the pressure in each fuel element would be as high as 52 atm.

The initial step of decladding will consist of lowering cropped fuel subassemblies into the decladder so that the bottoms of the fuel elements penetrate the cover salt and are immersed to a depth of a few inches in the zinc at 800°C. The bottom few inches of cladding dissolve, and the fission gases are vented. Next, the subassemblies are lowered so that the zinc covers the fuel-containing zone of the fuel elements completely and the rest of the cladding dissolves.

Six experiments were completed to simulate the effect of a sudden release of gas under pressure, as would occur in a decladding operation. In each of the initial two experiments, a stainless steel tube (0.25-in. OD by 10-mil wall by 5-in. length) with a sealed end was attached to a steel capillary tube with Swagelok fittings and was pressurized to 6.8 atm with argon. In one of these runs, three UO_2 pellets (0.21-in. dia by 0.25-in. length) were contained in the tube; in the other run, the tube was empty except for argon gas. The individual tubes were immersed through a 1/4-in. salt layer to a depth of 1 in. in the molten zinc bath at 800°C. The pressure within the tubes increased to about 9 atm. Gas

was released from one tube after 2.75 min. and from the other tube after 2.5 min. The release of gas from the tube that contained pellets was accompanied by the sound of the pellets hitting an interior surface of the crucible. Examination of the tubes after the experiments showed that 1 in. of the stainless steel had dissolved and that no expansion of the tube was apparent adjacent to the molten zinc-salt interface. There was evidence on the undissolved portion of the tubes that metal and salt had splashed to a height of about 5 in.

For each of the three subsequent experiments, a stainless steel tube (0.25-in. OD by 0.010-in. wall by 5.5-in. length) with the bottom end welded shut was charged with two (0.222-in. dia by 0.25 in. long) stainless steel rods and one rod of the same diameter but 4 in. long. By means of compression fittings and an additional length of 0.25-in.-dia tubing, each of the tubes loaded with rods was attached to a pressure gauge and a source of argon. The tubes were pressurized with argon, then a valve leading to the argon supply was closed. When a tube was lowered into the melt in the first of this series of experiments, the gas pressure within the tube increased from 22 atm to 25 atm in 1 min, then slowly decreased. Examination of the tube revealed that the wall had dissolved out to make a small opening above the welded end. The stainless steel rods remained in the tube.

The tube for the second of these experiments, with a pressure of ~45 atm, was partially immersed in the zinc. The pressure was 51 atm after 1.8 min, when pressure decreased suddenly and the rods hit the bottom of the graphite crucible. Examination of this tube revealed that its end was ruptured and flared out.

In the third experiment, the pressure in the tube, originally 46 atm, increased to 50 atm after partial immersion in the molten zinc. After 1.8 min, the gas vented rapidly from the tube through a hole in the tube wall similar to the hole observed in the first test with inserted steel rods. The rods remained in the tube in the third experiment.

Examination of the equipment after the third experiment showed that some zinc and salt had splashed to a height of about 19 in. (*i.e.*, to the top flange of the furnace). In the second experiment, the ejected steel rods had made a hole in the bottom of the graphite crucible. This projectile effect would not be harmful in an actual fuel subassembly decladding operation because heavy stainless steel hardware would occupy the area below the fuel elements at the rupture stage of decladding. However, because of its force, the gas escaping from the fuel element might eject zinc upward around the fuel elements inside the stainless steel shroud.

In the final experiment reported here, two fuel elements were simulated by stainless steel tubes (0.25-in. OD by 0.010-in. wall by 5.5-in. length) with the bottom end of each welded shut and each containing two short stainless steel rods (0.222-in. dia by 0.25 in. long) and one longer rod (0.222-in. dia by 4 in. long). These two tubes were each attached with compression fittings to an additional length of 0.25-in. dia tubing, a source of argon, and a pressure gauge (total volume of each gas reservoir was ~25 cm^3). The tubes were pressurized with argon to a 54-atm

pressure and the valve to the gas supply was closed, after which the tubes were fastened inside a 2-in.-OD stainless steel tube (simulating a shroud) that had a 5/8-in. opening in the bottom and was sealed at the top (Fig. 5). The top of the large tube was sealed from the atmosphere by a large Cenco fitting and by individual Veeco fittings for each of the two 0.25 in.-OD stainless steel tubes.

This assembly of the 2-in.-OD tube containing two 0.25-in. OD tubes was lowered to a depth of 3 in. into the zinc-salt melt, which was at 785°C. The 6-in. deep melt was contained in a graphite crucible (4 1/8-in. OD by 0.25-in. wall by 10 in. high) with a tantalum secondary (4 1/4 in. OD by 20-mil wall by 13 1/4 in. high). The crucible and secondary were further contained in a stainless steel crucible (15 3/4-in. OD by 1/16-in. wall by 15 1/4 in. high). Fiberfrax insulation was placed in the top portion of the annulus between the tantalum secondary and the stainless steel container. Heat shields attached to the top furnace flange fit inside the stainless steel container and rested on the top of the tantalum secondary. With this arrangement, there was about a 3-in. freeboard above the melt in the graphite crucible and an additional 3 1/4-in. height in the tantalum secondary. The heat shields diverted splashed salt and metal back into the graphite crucible and into the annulus between the graphite crucible and tantalum secondary.

When the assembly was immersed in the melt, the pressure in each tube increased from 54 atm to 61 atm. The pressure decreased slowly in one tube after 4.9 min; in the other tube, the pressure decreased rapidly after 5.7 min.

The 0.25-in.-OD stainless steel tubes were examined following the experiment. Uniform corrosion of the exposed surfaces had occurred, and the gas had escaped through small cracks in the wall of the tubes. The rods had remained intact inside the tubes. Some zinc had blown out of the graphite crucible and into the tantalum secondary, but this would not constitute a problem in plant equipment since splash shields would be incorporated into the equipment that would effect zinc containment in the crucible.

D. THE BEHAVIOR OF VOLATILE FISSION PRODUCTS

(M. Krumpelt, J. J. Heiberger, M. J. Steindler)

The control of volatile fission products will be a major problem in the reprocessing of high-burnup, short-cooled fast breeder fuel. The ^{131}I and ^{133}Xe contents of FBR fuel will be many times greater than in present LWR fuel. No reliable method has yet been demonstrated that can achieve the high removals of volatile fission products required in the reprocessing of irradiated FBR fuel. New solutions to the problem of iodine removal are being sought at the Oak Ridge National Laboratory,[3] and solutions to the problem of noble gas absorption are being sought at the

[3] W. E. Unger, R. E. Blanco, D. J. Crouse, A. R. Irvine, C. D. Watson, "LMFBR Fuel Cycle Studies Progress Report, No. 5 and 6," USAEC Reports ORNL-TM-2671 and -2710 (1969).

Figure 5

Simulated Fuel Assembly for Pressure Test

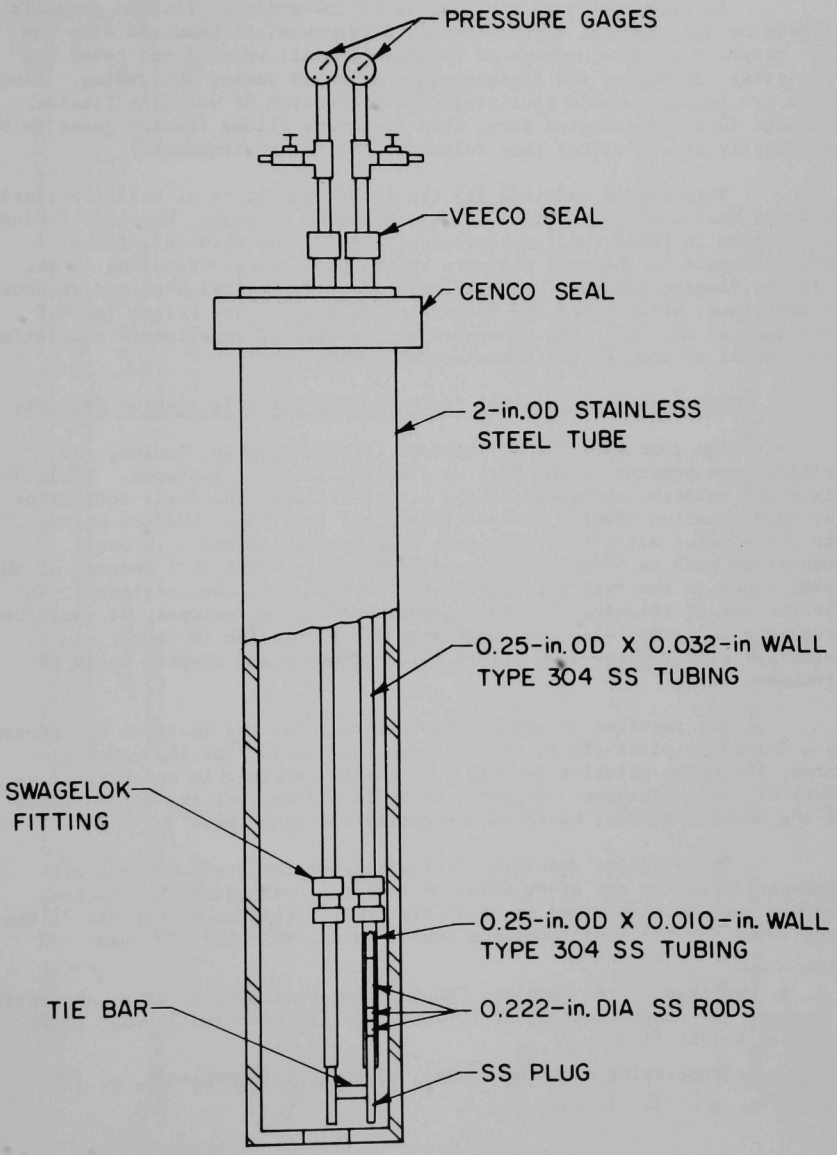

Gaseous Diffusion Plant.[4] The proposed processes would provide for plant off-gas being decontaminated and ultimately released into the atmosphere.

An alternative to the release of low-activity fission gases is offered by pyrochemical reprocessing. A pyrochemical head-end step has been proposed using equipment of relatively small volumes and cover gas consisting largely of the fission gases released during decladding. Since these two features would facilitate the collection of volatile fission products in a concentrated form, this procedure allows fission gases to be permanently stored rather than released into the environment.

This report examines (1) the total quantities of volatile fission products that must be handled, (2) the behavior of xenon, krypton, iodine, and tritium in LMFBR fuel reprocessing, and (3) the chemical states of these elements in the fuel elements before processing. Handling of the volatile fission products by chop-leach and pyrochemical head-end methods is described, briefly for the former method and in more detail for the pyrochemical method. Also presented are results of experiments simulating the removal of iodine in a pyrochemical system.

1. Quantities and Chemical States of the Volatile Fission Products

The four elements of interest (xenon, krypton, iodine, and tritium) are present in the fuel as a multiplicity of isotopes. Table 3 lists the relative abundance of the active isotopes and their activities for 30-day-cooled Atomics International (AI) fuel (51.5 MWd/ton burnup). The three major activities originate from isotopes present in small quantities such as ^{133}Xe, which constitutes only about 10^{-2} percent of the total xenon in the fuel but contributes most of the xenon activity. In the process of removing the small amounts of active isotopes, it would be necessary to remove also the large amounts of inactive isotopes. In a 5-ton/day plant, about 5500 liters (STP) of xenon and krypton would be processed daily.

The required decontamination factors for the isotopes of interest in a 5-ton/day plant (Table 4) have been calculated from the generation rates, the stack dilution factor, and maximum permissible concentrations (MPC) of these isotopes. Column 2 of Table 4 lists the generation rates of the major isotopes, based on the activities from Table 3.

The dilution resulting from mixing of the stack off-gas with atmospheric air is the stack dilution factor. Average stack dilution factors have been obtained for four different locations in the USA.[5] The mean value for the four locations, which is 3×10^{-7} sec m^{-3}, has

---

[4] J. R. Merriman, J. H. Pashley, "Engineering Developments of an Absorption Process for Concentration and Collection of Krypton and Xenon," USAEC Report K-1786 (1970).

[5] "Aqueous Processing of LMFBR Fuels," USAEC Report ORNL-4436, p. 171 (1970).

Table 3

Volatile Fission Product Content of Core Plus Axial Blanket, Atomics International FBR Fuel

(30-day-cooled; average burnup, 51.5 MWd/ton)[a]

Isotope	Half Life	Abundance (g atoms/1000 kg U+Pu)	Activity (Ci/1000 kg U+Pu)	Heat (W/1000 kg U+Pu)
^{3}H	12.26y	0.051	1.49×10^{3}	0.053
^{85}Kr	10.76y	0.48 (7.7%)[b]	1.59×10^{4}	25.6
Total Kr		5.73	1.59×10^{4}	
^{129}I	1.7×10^{7}y	4.01 (73%)	0.085	
^{131}I	8.05d	0.014 (0.25%)	2.18×10^{5}	898
^{132}I	2.26h	--	6.76×10^{3}	108
Total I		5.48	2.25×10^{5}	1006
^{131m}Xe	11.8d	9×10^{-4} (10^{-3}%)	9.77×10^{3}	9.5
^{133m}Xe	2.26d		19.3	
^{133}Xe	5.27d	3.5×10^{-3} (7×10^{-3}%)	1.17×10^{5}	126
Total Xe		49.8	1.27×10^{5}	135.5

[a] Taken from ORNL-4436, Appendix A.

[b] Atom percent of indicated isotope as part of total fission elements.

Table 4

Volatile Fission Product Generation Rate and Emission Limits for a 5 tons/day FBR Fuel Reprocessing Plant

Isotope	Generation Rate[a] (Ci/sec)	1/3 MPC[b] (μCi/ml)	Required Decontamination Factor	
			Current[c]	Anticipated[d]
^{3}H	0.076	6.7×10^{-8}	<1	34
^{85}Kr	0.81	10^{-7}	2.4	240
^{133}Xe	5.95	10^{-7}	18	180
^{129}I	4.3×10^{-6}	1×10^{-15}[e]	1.3×10^{3}	1.3×10^{5}
^{131}I	11.1	4.6×10^{-14}[f]	7×10^{7}	7×10^{8}

[a] Five tons fuel (4400 kg U+Pu) per day, fission product activity as shown in Table 3.

[b] From 10 CFR 20, Appendix B, Table II.

[c] Using an average stack factor of 3×10^{-7} sec/m^3 (ORNL-4436, p. 171).

[d] Decontamination factors that may have to be achieved in future FBR fuel reprocessing plants.

[e] Includes 700^{-1} for cow-milk-child chain and 10^{-1} for residence (see ORNL-4436, p. 169).

[f] Includes 700^{-1} for cow-milk-child chain.

considerable uncertainty attached to it since, at any particular plant site, the average stack dilution factor may be ten times greater or smaller than the mean value.

To calculate a decontamination factor (DF) for an isotope, the generation rate multiplied by the stack dilution factor was divided by one-third the maximum permissible concentration (MPC) in air.[6] (For continuous release, an environmental concentration that is one-third the MPC is presently acceptable.)

The DFs in column 4 of Table 4 are based on current MPCs (which are now being reviewed by the AEC). Since decontamination requirements are expected to be more rigorous for fuel processing plants 20 years hence, decontamination methods need to be developed that exceed present requirements. Column 5 of Table 4 lists DFs that may have to be achieved in the future. For the longer-lived isotopes ^{3}H, ^{85}Kr, and ^{129}I, it is anticipated that DFs will be a hundred times current DFs. For short-lived ^{131}I and ^{133}Xe, DFs only 10 times higher may be required. Table 4 shows that a very high DF will be necessary for iodine and that removal of the noble gases from off-gas may also have to be fairly complete.

The removal of volatile fission products requires information on their chemical states and their behavior in the fuel elements prior to and during processing.

a. Xenon and Krypton

Xenon and krypton produced during irradiation of reactor fuel leave the fuel matrix by diffusion or (at sufficiently high temperature) by bubble migration. Studies[7-9] of the distribution of fission products in irradiated UO_2-PuO_2 fuel elements indicated that between 50 and 80% of the xenon and krypton is in the plenum section of irradiated fuel elements. The fraction released from the fuel matrix is greater at higher burnups. During reprocessing of the fuel, all of the gas in the fuel element plenum is released in the shearing step or decladding step.

---

[6] "Standards for Protection Against Radiation," 10 CFR 20, Appendix B, Table 2.

[7] D. Geithoff, G. Karsten, and K. Kummer, "Irradiation Performance of Fast Reactor Fuels," Report EURFNR-423 (1967).

[8] K. Q. Bagley and D. M. Donaldson, "Fission Gas Release from Mixed Oxide Fuels," Plutonium 1965, A. E. Kay, M. B. Waldron, Eds., Chapman and Hall, London (1967), p. 1963.

[9] R. E. Shavdahl, M. D. Freshley, W. J. Barley, and S. Goldsmith, "Irradiation Properties of High Energy Rate Pneumatically Impacted UO_2-PuO_2 Fuels," Ibid., p. 1013.

b. Iodine

Iodine can exist in the fuel as elemental iodine, as CsI, or (near the cladding) as FeI_2. The formation of CsI is thermodynamically favored in the fuel environment, and since the fission yield of cesium is about eight times that of iodine, CsI is likely to form initially during irradiation.

Further changes in the chemical form of iodine in the fuel during irradiation are controlled by a complex equilibrium involving the O/M ratio of the fuel and the burnup. The initial O/M ratio of the fuel is less than 2 but increases with burnup. In hypostoichiometric UO_2-PuO_2, oxygen has a very negative partial molar free energy, ranging between -160 and -140 kcal/mol (O_2). A very drastic change of about 80 kcal/mol occurs between O/M ratios of 1.99 and 2.01.[10] In hyperstoichiometric fuel, the oxygen potential approaches -50 kcal/mol.

The effect of burnup on the O/M ratio and, in turn, on the oxygen potential has been calculated by I. Johnson.[11] If the initial O/M ratio is 1.97, the fuel becomes hyperstoichiometric at a burnup of 5%. According to Johnson, the formation of Cs_2O or Cs_2UO_3 is thermodynamically possible in hyperstoichiometric fuel. CsI would then decompose to liberate iodine by a reaction similar to

$$2\ CsI + O_2 + UO_2 \rightleftarrows Cs_2UO_4 + I_2$$

Thus, it is anticipated that at high burnp, most of the iodine would be elemental.

In irradiated fuel elements, iodine has been observed to interact with the cladding, forming FeI_2.[12] The extent of the interaction in a high-burnup fuel is presently not known and is difficult to predict.

c. Tritium

The chemical state of tritium in a fuel element is also related to the burnup and the initial O/M ratio of the fuel. At very negative oxygen potentials, elemental tritium is thermodynamically stable, but in hyperstoichiometric fuel at higher burnup ^3H_2O may form.

---

[10] T. L. Markin and E. J. McIver, "Thermodynamic and Phase Studies for Plutonium and Uranium Oxides with Application to Compatibility Calculations," Ibid., p. 845.

[11] "Reactor Development Program Progress Report," USAEC Report ANL-7705, p. 166 (1970).

[12] C. E. Johnson, C. E. Crouthamel, J. Nucl. Mat. 34, 101 (1970).

The amount of tritium still in a fuel element when it is declad is affected by its rate of permeation through stainless steel cladding. Only minor quantities of tritium diffuse out of LWR fuel, probably because an oxide diffusion barrier forms on the outside of the cladding by a cladding-water reaction. No such layer forms on the cladding in a sodium-cooled reactor. In sodium-cooled EBR-II, operation is at a low enough temperature so that in the metallic fuel uranium tritide formation is favored. Hence, the tritium behavior in EBR-II is not typical of that for future fast reactors.

For the reference cladding material, Type 316 stainless steel, no exact information is available on the permeation coefficient of tritium. An estimate of the permeation coefficient has been calculated, as described below, by relating the isotope effect to the permeation coefficient of hydrogen through Type 316 stainless steel. Hydrogen permeation through Type 316 stainless steel at 600 and 700°C was measured at Knolls Atomic Power Laboratory[13] and at Oak Ridge.[14] These data are given in Table 5. The isotope effect can be calculated from permeation measurements that were made with both hydrogen and tritium in Type 347 stainless steel.[15] The ratio of the permeation coefficient of tritium to that of hydrogen is the isotope effect. Its value is 0.63 ± 0.03. If this correction factor is applied to the average of the two permeation coefficients of hydrogen at 600°C (Table 5), a permeation coefficient of tritium for Type 316 stainless steel of about 0.065 cm^3 (STP) mm cm^{-2} hr^{-1} $atm^{-1/2}$ is obtained at 600°C.

This calculated permeation coefficient has been used to estimate the permeation rate of tritium at 600°C through the cladding of an Atomics International core-and-axial-blanket fuel pin. The cladding has an area of approximately 490 cm^2 and is 0.45 mm thick; the plenum volume is 33 cm^3; the actinide content of a fuel element is 280 g. The tritium content after 30-day cooling would be 7×10^{-6} mol, which would correspond to a partial pressure of about 12 Torr at 600°C. For the purpose of this rough estimate, the permeation equation

$$Q = \beta \frac{A}{d} \sqrt{p}\, t$$

may be used where Q = permeating volume (STP), β = permeation coefficient, A = area (cm^2), d = thickness of membrane (mm), p = pressure (atm), t = time (hr). The permeation rate at 600°C and 12 Torr pressure through

---

[13] P. S. Flint, "The Diffusion of Hydrogen Through Materials of Construction," USAEC Report KAPL-659 (1951).

[14] H. W. Savage, E. L. Compere, R. E. MacPherson, W. E. Huntley, and A. Taboada, "Snap-8 Corrosion Program Quarterly Progress Report," USAEC Report ORNL-3784 (1964).

[15] D. Randall and O. N. Salmon, "The Permeability of Type 347 Stainless Steel to Hydrogen and Tritium," USAEC Report KAPL-904 (1953).

Table 5

Permeation Coefficients of Hydrogen Through Type 316 Stainless Steel

	β [cm^3(STP) mm cm^{-2} hr^{-1} $atm^{-1/2}$]	
Temp (°C)	KAPL-659	ORNL-3784
600	0.12	0.096
700	0.31	0.28

a cladding of the given dimensions is 6 cm^3 (STP) hr^{-1}. Since the total tritium content of the fuel element corresponds to a volume of only 0.16 cm^3 (STP), essentially no tritium will be retained in the plenum. We conclude that most of the tritium will permeate out of the fuel elements during irradiation and the 30-day cooling period and that fuel reprocessing operations will probably deal with only a small amount of tritium.

2. Handling of Volatile Fission Products

a. Chop-Leach Head-end

The head-end step generally employed in reprocessing commercial LWR fuel is chop-leach.[5] In chop-leaching, the fuel elements are chopped into small lengths, the fuel oxide is dissolved in acid for aqueous processing, and the cladding shells are disposed of as waste. Three characteristics of LMFBR fuel make processing by chop-leach methods problematic:

1. High heat generation, necessitating cooling of LMFBR fuel at the shear,

2. Incomplete dissolution of LMFBR fuel in HNO_3, due to its high plutonium content and high fission product content,

3. High activity of the fission gas.

To alleviate the problem related to high activity of the fission gas, voloxidation of the sheared fuel segments has been proposed.[5] With this modified chop-leach head-end, volatile fission products would be released at three points: at the shear, the voloxidizer, and the dissolver. The activity released at each point would be greater than the total fission-gas activity in LWR fuel. The three off-gas streams could be managed by two alternative procedures: (1) a separate decontamination system could be built for each stream, or (2) the streams would be combined and treated jointly. If joint treatment is selected, the gas to be decontaminated would consist of the fission gases and the following:

1. A hopefully moderate volume of purge gas from the shear. (It is planned to use separate systems for purging the sheared fuel and cooling the unsheared fuel, although no provision for a seal between the systems has yet been reported.)

2. A large quantity of gas, primarily oxygen, from the voloxidizer.

3. An unspecified quantity of purge gas (probably nitrogen saturated with water and nitrogen oxides) from the dissolver.

The total off-gas volume would be large; decontamination of this complex gas mixture would be a formidable task.

b. Pyrochemical Head-end

An alternative to chop-leach is a pyrochemical head-end such as the conceptual process described in ANL-7735, pp. 26-33. It consists of liquid-zinc-decladding and fuel-reduction steps. In this process, volatile fission products would be released from the fuel during both decladding and fuel reduction, but the bulk would be released from the fuel element plenum during decladding. Both of the pyrochemical head-end steps would be conducted in the same closed furnace compartment, and 100% of the fission gases would vent into the space above the crucible, becoming constituents of the cover gas. The cover gas would consist largely of noble-gas fission products, which would largely be stable isotopes (Table 3). A relatively small input of argon to the cover gas would occur in the conceptual process when a turret for transferring fuel subassemblies to the decladding furnace is evacuated into the cover-gas system (just before the turret is disconnected from the furnace compartment). A computation has shown that the average composition of the gas, if homogenized AI fuel were processed, would be 64% Xe, 29% Ar, and 7% Kr.

A schematic of a conceptual cover-gas handling system is shown in Fig. 6. Gas from the furnace compartment passes through a filter and cooler and is then pumped into an intermediate storage tank. From the tank, it may be returned to the furnace compartment. The desired cover-gas pressure in the furnace compartment is maintained by automatically regulated additions and withdrawals of gas. Excess gas is ultimately pumped from the intermediate storage tank into permanent storage tanks, which are standard gas cylinders. Nine such cylinders containing gas at 225 psi would accommodate the total daily off-gas from a 5-ton/day plant. The gas could be stored indefinitely in the cylinders, or the noble gas content could be fractionated and the xenon sold after ^{133}Xe has decayed. Fission product iodine released during a pyrochemical head-end step does not become a constituent of the cover gas but is retained completely in the molten salt (see below). Little tritium is expected to remain in the fuel for release during decladding, as discussed above, but any tritium released would probably accompany xenon and krypton to the permanent storage cylinders.

(1) Control of Iodine

The behavior of iodine in a pyrochemical head-end is difficult to predict because of uncertainty about the chemical state of iodine in the fuel. The theoretical arguments presented above suggest that most of the iodine would be in the elemental form. If iodine accumulates in the plenum of fuel elements, it will be ejected into the liquid zinc with xenon and krypton when the stainless steel cladding ruptures during decladding. The gas bubbles will rise upward through the liquid zinc and the molten cover salt, and ultimately merge into the cover gas.

Two types of experiments were performed to simulate the release of iodine fission gas during decladding and to investigate the degree of zinc-iodine interaction. In the first type of experiment, iodine was released into a pool of zinc when an iodine-containing capsule ruptured; in the second type, iodine was bubbled through a zinc pool.

Figure 6

Conceptual Cover-Gas Handling System

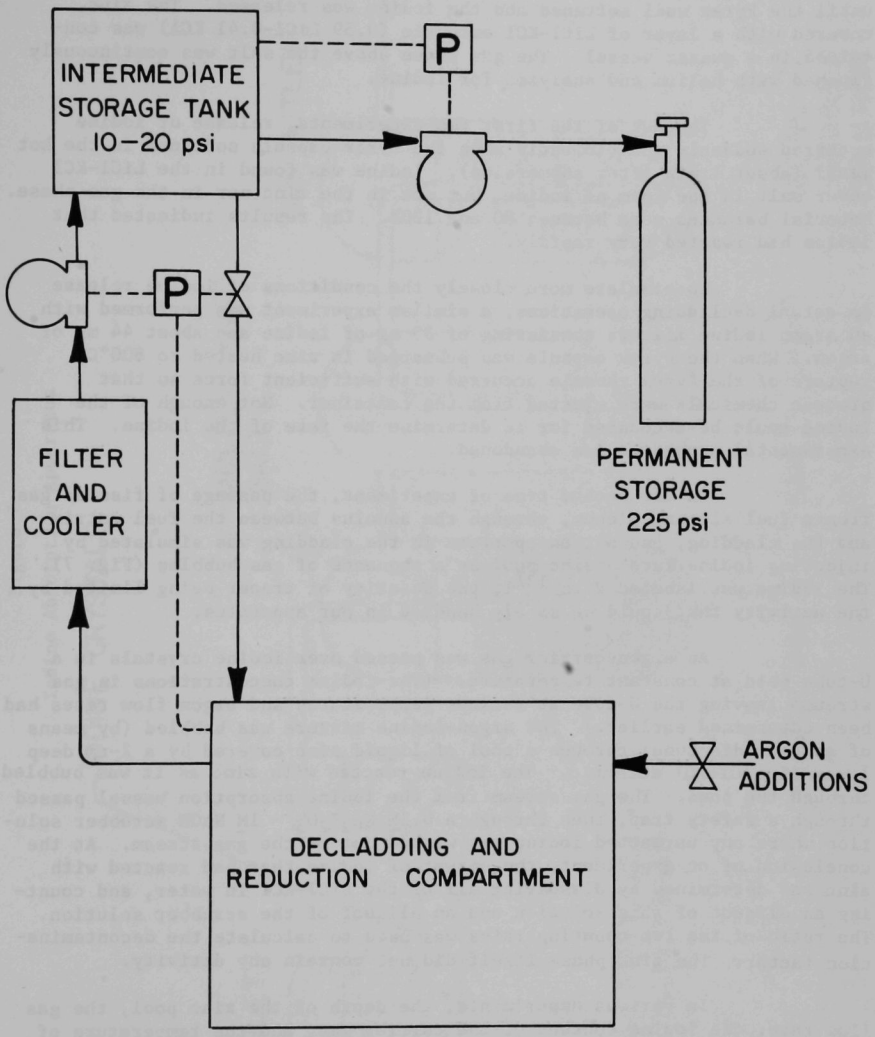

Initial experiments of the first type utilized elemental iodine sealed in Pyrex capsules. An iodine-containing capsule was submerged (by a remotely operated mechanism) in a pool of zinc held at 800°C until the Pyrex wall softened and the iodine was released. The zinc, covered with a layer of LiCl-KCl eutectic (0.59 LiCl-0.41 KCl) was contained in a quartz vessel. The gas phase above the salt was continuously flushed with helium and analyzed for iodine.

In each of the first two experiments, release of iodine occurred suddenly and violently when the Pyrex capsule softened in the hot metal (about 1 min after submersion). Iodine was found in the LiCl-KCl cover salt in the form of iodide, but not in the zinc nor in the gas phase. Material balances were between 80 and 120%. The results indicated that iodine had reacted very rapidly.

To simulate more closely the conditions of iodine release in actual decladding operations, a similar experiment was performed with an argon-iodine mixture consisting of 33 mg of iodine and about 44 mg of argon. When the Pyrex capsule was submerged in zinc heated to 800°C, rupture of the Pyrex capsule occurred with sufficient force so that process chemicals were ejected from the container. Not enough of the iodine could be accounted for to determine the fate of the iodine. This experimental procedure was abandoned.

In the second type of experiment, the passage of fission gas from a fuel element plenum, through the annulus between the fuel matrix and the cladding, and out an aperture in the cladding was simulated by injecting iodine into a zinc pool as a sequence of gas bubbles (Fig. 7). The iodine was labeled with ^{131}I, the quantity of tracer being limited by the activity that could be safely handled in our apparatus.

An argon carrier gas was passed over iodine crystals in a U-tube held at constant temperature. (The iodine concentrations in gas streams leaving the U-tube at various temperatures and argon flow rates had been determined earlier.) The argon-iodine mixture was bubbled (by means of an 8-mm dia tube) through a pool of liquid zinc covered by a 2-cm deep layer of LiCl-KCl eutectic. The iodine reacted with zinc as it was bubbled through the pool. The gas stream from the iodine absorption vessel passed through a safety trap, then through a 0.1$\underline{M}$ $Na_2S_2O_3$ - 1$\underline{M}$ NaOH scrubber solution where any unreacted iodine was washed out of the gas stream. At the conclusion of an experiment, the amount of iodine that had reacted with zinc was determined by dissolving all of the LiCl-KCl in water, and counting an aliquot of this solution and an aliquot of the scrubber solution. The ratio of the two counting rates was used to calculate the decontamination factor. The zinc phase itself did not contain any activity.

In various experiments, the depth of the zinc pool, the gas flow rate, the iodine content of the carrier gas, and the temperature of the zinc were varied. The experimental parameters and results are listed in Table 6.

The counting rate for the aqueous scrubber solution never exceeded background. As a result, the decontamination factors (DFs) in

Figure 7

Iodine Absorption Apparatus

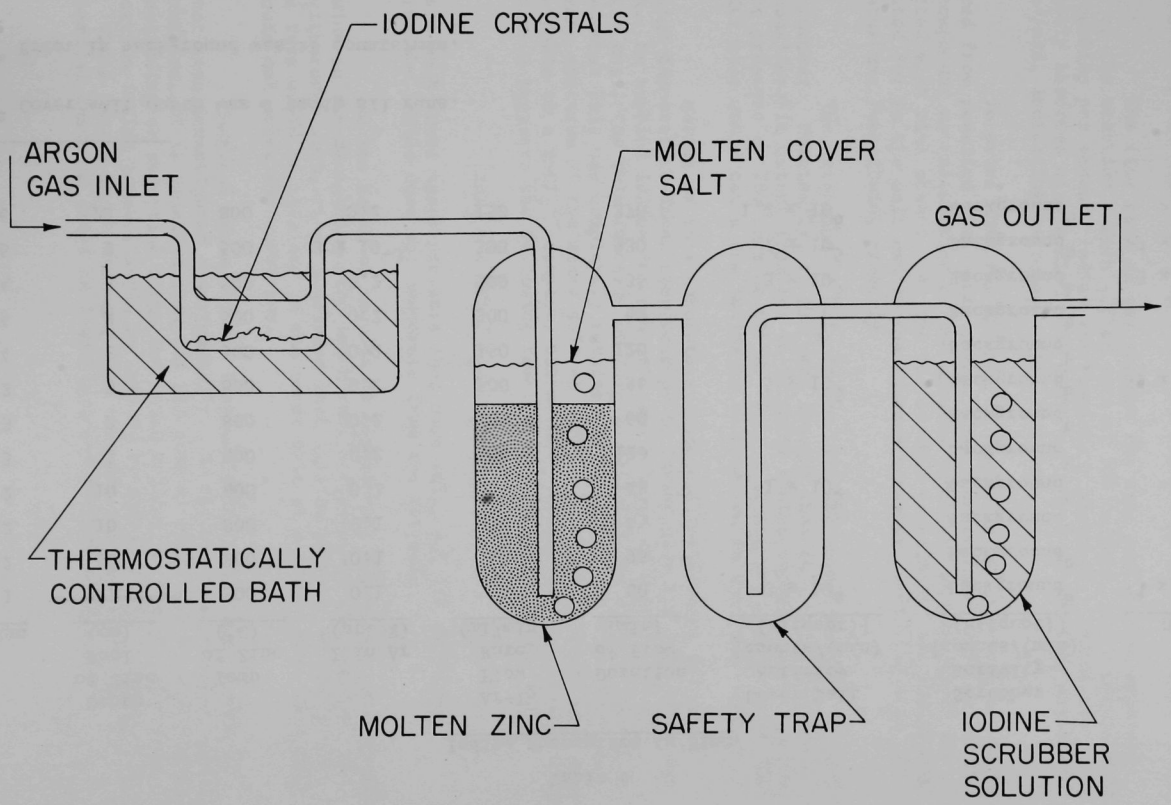

Table 6

Iodine Absorption in Zinc

Run	Depth of Zinc Pool (cm)	Temp of Zinc (°C)	I in Ar (at. %)	$Ar-I_2$ Flow Rate (ml/min)	Duration of Flow (min)	Cover Salt Activity [counts/(min) (aliquot)]	Scrubber Activity [counts/(min) (aliquot)]	DF
1	17	500	0.1	65	60	3×10^4	Background[b]	$>3 \times 10^3$
2	10	800	0.1	65	95		Background[b]	
2	10	800	0.1	150	45		Background[b]	
2	10	800	0.2	150	48	1×10^5	Background[b]	$>10^4$
3	3	800	0.2	150	120		Background[b]	
3	3	800	0.2	300	60		Background[b]	
3	3	800	0.2	500	36	5×10^5	Background[b]	$>5 \times 10^4$
4	3	500	0.2	150	120		Background[b]	
4	3	500	0.2	300	60		Background[b]	
4	3	500	0.2	500	36	3×10^5	Background[b]	$>3 \times 10^4$
5	3	500	3×10^{-3}	300	330	7×10^5	Background[b]	$>7 \times 10^4$
6	10	800	0.2	150	370	1.2×10^6	Background[b]	$>10^5$

[a] Cover salt depth was 2 cm in all runs.

[b] Error in background was ±8 counts/min.

the right-hand column of Table 6 are not equilibrium values but lower limits, indicating that possibly higher Dfs can be reached in apparatus radiologically safe for handling iodine of higher specific activity.

The flow rate of gas through the zinc pool had no apparent effect on the reaction. With a flow rate of 500 cm^3/min, which corresponded to 70 bubbles per second, iodine was completely absorbed. Iodine was completely absorbed with a zinc pool depth of only 3 cm and flow rates of 500 cm^3/min, indicating extremely rapid reaction.

To prove that the absence of counts in the scrubber solution resulted from reaction with zinc, rather than from reaction with an equipment component or malfunction of the aqueous scrubber, an experiment was conducted with zinc absent. At the end of this experiment, all iodine was accounted for in the salt and in the aqueous scrubber, verifying that the apparatus was functioning properly.

The retention of ZnI_2 in the LiCl-KCl cover salt was investigated further. Originally, it had been thought that ZnI_2 might evaporate to a considerable extent from the Zn-LiCl-KCl system because pure ZnI_2 has a vapor pressure of 760 Torr at 625°C. Only a strong interaction with the LiCl-KCl salt would cause the iodine to be retained in the 800°C system.

Maroni of this Laboratory (Chemical Engineering Division) used high-temperature Raman spectroscopy to investigate the type of interaction. He bubbled iodine through zinc and a layer of molten LiCl-KCl eutectic until the mole fraction of ZnI_2 in LiCl-KCl was 0.05, it being assumed that ZnI_2 was completely retained in the salt. He then recorded the Raman spectrum of the mixed salt at 450°C. The only observed peak was attributable to a $ZnCl_4^{2-}$ complex, but no ZnI_2 vibrations were found. This observation suggests the following reaction between ZnI_2 and LiCl-KCl:

$$ZnI_2 + 4\ KCl \rightleftarrows K_2ZnCl_4 + 2\ KI.$$

KI has a much lower vapor pressure than does ZnI_2, and its formation explains why iodide does not evaporate from the hot salt.

On the basis of results of experiments simulating the release of iodine in the decladding step and Maroni's finding on the reaction of ZnI_2 with cover salt, it is concluded that fission product iodine in elemental form would be retained in the cover salt of a liquid zinc decladder and would not enter the cover gas.

Chemical states of the fission iodine other than elemental have not been investigated experimentally. On the basis of free energies of formation, it is expected that any CsI present would not be affected in the decladding or reduction steps but would collect in the chloride salt. Any ferrous iodide present would be reduced by metallic zinc to ZnI_2 and iron. These data suggest strongly that adequate control of iodine in pyrochemical head-end steps is feasible under process conditions.

II. CONTINUOUS CONVERSION OF U/Pu NITRATES TO OXIDES

(N. M. Levitz, D. E. Grosvenor, S. Vogler, F. G. Teats, R. V. Kinzler)

In the preparation of LMFBR fuel, uranium-plutonium nitrate solutions produced in reprocessing plants must be converted to powdered fuel oxides suitable for the fabrication of fuel shapes. The high rates of plutonium throughput needed for LMFBR fuel recycle necessitate equipment of large capacity. The problems of nuclear criticality and self-irradiation associated with plutonium provide an incentive for developing continuous processes and equipment so that a large capacity can be achieved with a relatively low plutonium holdup.

A fluidized-bed conversion process based on technology developed in earlier ANL fluidization work[1] is under development here for producing (1) either uranium-plutonium oxide or plutonium oxide that could be mechanically mixed with uranium oxide for fabrication into fast reactor fuel and (2) powdered plutonium oxide, which could be shipped more safely and in smaller volumes than the nitrate solutions currently being shipped. Basic process steps include fluidized-bed denitration of uranium-plutonium nitrate solutions to UO_3-PuO_2 powder, followed by fluidized-bed reduction with hydrogen to UO_2-PuO_2. Pilot-scale and laboratory-scale work is in progress.

Initial results of drop-denitration laboratory experiments on the conversion of U-20% Pu nitrate to oxide and the development of an oxide-dissolution procedure for the pilot plant program were described in the preceding report (ANL-7735) in this series. Good distribution of PuO_2 in the UO_3 matrix was noted. The pilot-scale fluidized-bed reactor and associated equipment were also described, as was the process. In this report, the results of laboratory work on the stability of plutonium ions in solution and a summary of the shakedown operations in the pilot plant with uranium feed solutions are presented.

A. LABORATORY PROGRAM

1. Stability of Plutonium Ions in Solution

The change in valence distribution of plutonium ions in nitrate solutions with time was measured by spectrophotometric examination of a 3M HNO_3 solution containing 1.35M plutonium. This solution was sampled periodically, and the amounts of Pu(VI) and Pu(IV) were calculated from the optical spectra.

Figure 1, which presents our results along with data from Atlantic-Richfield, Hanford,[2] for 5.3M HNO_3 solution containing 0.82M Pu, shows a straight line for the concentration of Pu(VI) as a function of time for the early part of the reaction, indicating a zero-order reaction with respect to the Pu(VI) concentration. The slopes for the two plutonium

---

[1] A. A. Jonke, E. J. Petkus, J. W. Loeding, and S. Lawroski, Nucl. Sci. Eng. 2, 303 (1957).

[2] D. T. Crawley, "Pressure Buildup of Plutonium Nitrate Solutions in Sealed Shipping Containers," ARH-1093 (July 15, 1969).

Figure 1

Reduction of $Pu(VI)$ in HNO_3

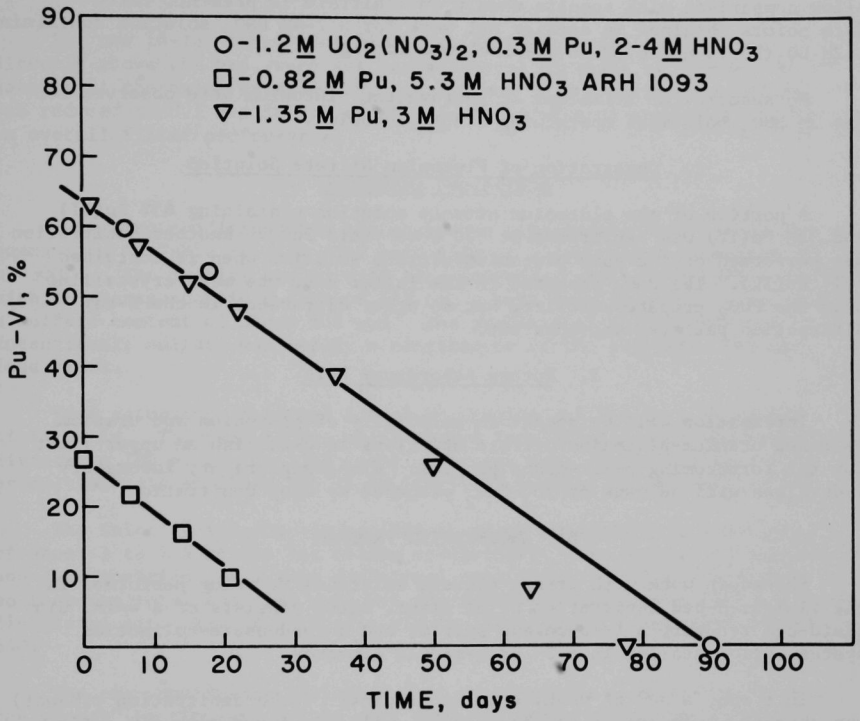

solutions are similar, indicating that the rate of valence change is independent of the initial plutonium concentration in this range. After about 50 days, the rate of reaction in the ANL solution increased. To allow comparison with results when uranyl nitrate is present, three data points obtained in earlier ANL work for a 2-4M HNO_3 solution containing 1.2M $UO_2(NO_3)_2$ and 0.3M Pu are included in Fig. 1.

No spectra for trivalent or pentavalent plutonium were observed for the 3M HNO_3 solutions containing 1.35M plutonium.

2. Denitration of Plutonium Nitrate Solution

A portion of the plutonium nitrate solution containing 65% Pu(VI) and 35% Pu(IV) was denitrated at 300°C to yield PuO_2. Another denitration was performed on the same plutonium nitrate solution when it contained only Pu(IV). The PuO_2 prepared in the latter case was more crystalline than the PuO_2 prepared earlier, but no other difference in the X-ray diffraction patterns was apparent.

3. Future Laboratory Work

Information will be sought on solubility of plutonium and uranium in mixed uranium-plutonium nitrate solutions to establish an upper limit for the forthcoming pilot-plant program. Also, exploratory laboratory reductions will be made of UO_3-PuO_2 prepared by drop denitration.

B. ENGINEERING PROGRAM

Shakedown work with uranyl nitrate solutions is being performed in the fluidized-bed denitration pilot plant, which consists of a 4-in. dia fluid-bed reactor, a feed-makeup system, and a condensate-collection system, all installed in a 3- by 4-module glovebox.

In a run, a bed of uranium oxide (typical of the denitration product) was charged, then heated to about 300°C while fluidized with air. Air was initially fed to all lines opening into the reactor (i.e., the liquid and air sides of the two-fluid feed nozzle for atomizing the nitrate feed solution, the product-withdrawal overflow line, and the pressure taps). After a few minutes operation at temperature, a stream of water was substituted for air in the liquid side of the spray nozzle, which was installed 9 in. above the reactor base. When the bed temperature was stabilized, feeding of water was stopped and a solution of uranyl nitrate was sprayed into the bed. Either the liquid uranyl nitrate droplets wet the bed particles, thermally decomposed, and deposited a fresh oxide layer, or the droplets decomposed in the gas phase and formed solid particles.

In the original setup, product solids overflowed continuously into a side takeoff line (a purged 1/4-in. IPS sidearm welded at a 45° angle, 12 in. above the flanged bottom). This product withdrawal system was modified in run U-6 because of an inability to control bed inventory. One change was the use of the cone bottom as an auxiliary product takeoff point, i.e., the solids were withdrawn countercurrently to the fluidizing-gas stream at the cone apex (a 1-in. IPS opening). Product removal through

the overflow system was continuous; product takeoff at the bottom was intermittent (through a valve). A further modification under consideration is an overflow pipe of larger diameter, with the solids takeoff rate controlled partly by the flow of purge air.

The two 18-in. long, sintered metal filters, which are mounted directly above the bed, were set for automatic blowback at 20-min intervals; the pulse duration, 0.5 to 1.0 sec in the early experiments, was reduced to 0.1 sec in the final experiment with no observed effects on overall filter performance.

1. Operating Conditions

Operating conditions for the shakedown experiments (U-1 to -6) are summarized in Table 1. All runs were made at a denitration temperature of 300°C. The initial bed in each case comprised about 7200-8500 g of UO_3 with an average particle size of 162 μm, a bulk density of 4.2 g/cc, and a sulfate content of about 800 ppm. The presence of sulfate was not intentional; sulfate was merely a constituent of the available bed and feed stock.

Feed solutions contained 1 to 2.4M uranium and 0.2 to 1.0M excess nitric acid. The feed rates, which ranged from 50 ml/min of 1M uranyl nitrate to 100 ml/min of 2.4M uranyl nitrate, were equivalent to a production rate of 22 to 105 lb UO_3/(hr)(ft^2 reactor cross section).

The inlet fluidizing air was fed at rates equivalent to a velocity of about 1 to 1.5 ft/sec (at column conditions). Air fed at the nozzle and decomposition gases were additional constituents of the gas stream so that the total gas flow rate was approximately double that of the fluidizing air. Ratios of nozzle air to liquid in the feed were 330 to 640.

The six experiments performed this quarter were carried out "through the gloves" to simulate future work with plutonium-containing materials. Exploratory runs were made over a wide range of operating conditions to determine any particle-size effects (e.g., growth or diminution trends in bed particle size).

2. Results

Runs were judged on the bases of mechanical operability, ease of startup and shutdown, ability to maintain uniform feed rate and fluidized-bed level, and sufficient heat input capacity for the design goal of 100 lb UO_3/(hr)(ft^2). Results were generally good except in run U-2, which was terminated within one hour of startup when a large temperature spread and unusual bed differential pressure fluctuations were observed. The bed was found to be agglomerated virtually into a single mass, but the cause was not determined. The duration of other runs was 3 to 14 hr.

Data were obtained on elutriation of fines (-200 mesh) from the bed, fines formation, particle growth (increase in average bed particle size), and the formation of agglomerates (+8 mesh). Results are considered preliminary and conclusions tentative because runs were of relatively

Table 1

Operating Conditions for Shakedown Experiments in Denitration Pilot Plant

Denitration Temperature: 300°C

Run No.	Run Duration (hr)	Starting Bed Weight (g)	Fluidizing Air Velocity (ft/sec)	Feed Solution Composition (M) U	Feed Solution Composition (M) Excess HNO_3	Feed Rate (ml/min)	Ratio of Nozzle Air to Liquid [scfm/(cc-min^{-1})]	Duration of each Blowback Pulse (sec)
U-1	3	7244	1	1	1	50	-	0.5
U-2	2/3[a]	7318	1	1	1	100	-	0.5
U-3	10[b]	7678	1.5	1	1	75-100	500-640	0.5
U-4	14	7847	1.5	2.4	0.3	60-100	480-520	0.5-1.0
U-5	9.4[c]	8495	1.4	2.0	0.2	80-107	330-480	0.5-1.0
U-6	6	∿8400	1.2	2.1	0.4	80	465	0.1

[a] Unscheduled shutdown because the bed became agglomerated; reason not known.

[b] Unscheduled shutdown because of plugged product overflow line.

[c] Unscheduled shutdown because of fines buildup on the sintered metal filters, resulting in excessive filter pressure drop.

short duration, and since results for uranium-plutonium systems may differ from those for uranium alone.

Fines were elutriated from the initial charge of UO_3. The bulk of the fines produced during denitration apparently were elutriated also and accumulated on the filters. This was determined from sieve analyses of grab samples of product collected at half-hour intervals and from the observed increases in differential pressure across the sintered-metal filters (an indication of fines buildup). Fines production, which represented about 5% of the total UO_3 production, appeared to be a function of feed rate.

With the existing column, it would be difficult to return fines to the bed and ultimately withdraw them with the bulk product during a run since the gas velocities above the bed are relatively high. The combined fluidizing gas, atomizing air, and decomposition gases give a linear gas velocity of about 3 ft/sec. Blowback pulse durations in the range 0.1 to 1.0 sec were employed at the sintered metal filters with about equal success in momentarily releasing the filter cake, but the material apparently did not recombine with the bed.

One solution would be to collect the fines separately by offsetting the filter section. An alternative solution would be to use a cyclone separator. The fines could be combined with the bulk product and treated further as needed (e.g., reduced with hydrogen in the case of a UO_3-PuO_2 product). The quantities of fines produced to date are within an acceptable range for use in subsequent fluidized-bed reaction steps.

Slight particle growth in the bed was evident from sieve analyses of product samples taken at half-hour intervals. Product sampled at the overflow point and at the bottom withdrawal point had similar particle growth patterns and comparable particle-size distributions, an indication of good mixing in the bed. From work to date, it cannot be predicted whether the growth trends would continue or whether a steady-state particle-size distribution would be attained. Demonstration runs of long duration would provide information on this question.

Examination of the final bed after each run (except experiment U-6) disclosed that coarse (+8 mesh) particles had accumulated in the cone bottom. About 5 to 10% of the total UO_3 produced in a given run consisted of coarse particles. Their manner of formation is not known, and their presence apparently did not influence the course of the runs; nevertheless, continual withdrawal of this fraction seemed desirable.

Bottom takeoff of product, instituted in run U-6 to allow withdrawal of coarse particles, was only partially successful. Bridging occurred in the cone opening, and about 1100 g of +8 mesh UO_3 (equivalent to about 7% of the total UO_3 produced) was in the reactor at the end of the run. Bridging, believed to have occurred early in the run, did not interfere with the withdrawal of free-flowing bed material throughout the run.

Coarse material can probably be withdrawn if the opening at the cone apex is enlarged. This material would be recycled to a feed makeup system or ground for feeding to the reduction step along with the bulk

product.

If the problem persists in the uranium-plutonium program, the reasons for formation of coarse material will be sought. A current hypothesis is that the proximity of the opposite wall to the feed nozzle (a distance of 4 in.) is a contributing factor. Use of a column of larger cross section (e.g., a 4-in. thick slab greater than 4 in. in width) might solve this problem. Tests with slab-shaped columns are within the scope of this study.

The experiments made this quarter provided valuable training for personnel. The throughput and operability potential of the equipment were demonstrated and a design goal of 100 lb UO_3/(hr)(ft^2 reactor cross section) was reached.

C. FUTURE WORK

Since the effect of a given variable in work with uranium alone may not be the same as for mixed uranium-plutonium systems, only a limited amount of work will be done with uranium. Work with uranium-plutonium is now being planned. Critically safe auxiliary items (e.g., a dissolver to permit recycle of UO_3-PuO_2 and a feed storage vessel) are being designed. Some modifications of the glovebox are also needed prior to work with plutonium.

Work at Idaho Nuclear Corp. with 4-in. and 6-in. dia fluidized-bed denitration units is being monitored. Direct comparison of Idaho work with our denitration results for uranyl nitrate feed solution should be possible.

III. IN-LINE ANALYSIS IN FUEL FABRICATION

(J. G. Schnizlein, M. J. Steindler)

Reduction of the cost of fuel fabrication is necessary to improve the competitive economic position of power-producing nuclear reactors. Large-capacity fabrication plants will require rapid, automated, and perhaps continuous in-line analytical methods.

In the absence of experimental data relating the effects of various fuel properties to fuel performance, rigorous specifications for ceramic FBR fuel have been set. As a result, analytical methods and their application to the fabrication process and products have become important factors in the economics of the fuel cycle. It is necessary to develop analytical methods capable of determining the physical and chemical properties of the fuel with the precision and accuracy necessitated by the relationship between fuel performance and properties of the as-charged fuel.

A. FUEL PROPERTIES

Uranium-plutonium oxides are the furthest developed ceramic fuels and consequently are expected to fuel the first commercial FBR. The specifications and required precisions for Fast Flux Test Facility (FFTF) fuel[1] are being used initially as the criteria in considering alternative and potential in-line fuel-fabrication analytical methods. The fuel properties selected for initial study (because their determination is a part of any conceivable fabrication procedure) are the uranium/plutonium ratio and the oxygen/metal ratio. The specifications, precisions, and acceptable methods of measurement[2] of these two properties have been discussed in the preceding quarterly report, ANL-7735.

B. URANIUM/PLUTONIUM RATIO IN FUEL

X-ray fluorescence analysis is being evaluated as an in-line analytical method for determining uranium/plutonium ratio in FBR fuel. This is a sensitive, nondestructive method in which exciting radiation (e.g., from an X-ray tube) impinges on the sample and causes the emission of radiation that is characteristic of the elements present; by this method, uranium and plutonium concentrations can be determined rapidly and accurately.

Analysis of the uranium and plutonium content of oxide by X-ray fluorescence is routinely practical to a relative precision of about ±2%. At other sites, X-ray fluorescence has been applied to analyzing (U,Pu) nitrate solutions, both inactive samples[3] and samples from process

---

[1] C. A. Strand, Pacific Northwest Laboratory, private communication, Feb. 1969 (summarized in ANL-7735).

[2] "Analytical Chemistry Methods in Support of Driver Fuel Fabrication," BNWL-1024 (Oct. 25, 1968).

[3] D. Ertel, Simultaneous Determination of Uranium and Plutonium by X-ray Fluorescence, J. Radioanal. Chem. 2, 205-9 (1969).

streams[4] containing radioactivity. The relative standard deviation,[3] taking the background count into account, for solutions containing up to 10 mg U/ml and 3.5 mg Pu/ml was observed to approach ∿0.6%.

The most rigorous specification on plutonium content for the FFTF, which is a precision of ±0.5% for the core zone, requires a greater sensitivity and efficiency than is routinely available. To attain this precision in the analysis of solid oxide as powder or pellets, matrix effects due to high absorption coefficients, crystallite size, scattering by voids and surface roughness, and enhancement (secondary fluorescence) must be proved to be insignificant or measurable. In this experimental program to demonstrate the practicality of analysis, it is planned to define not only the above material effects but also instrumental choices and sample presentation procedures. The required degree of precision also necessitates careful attention to counting statistics.

Development of an X-ray fluorescence method is proceeding, with thorium being used as a stand-in for uranium and uranium as a stand-in for plutonium. ThO_2-UO_2 can be used as a stand-in for UO_2-PuO_2 because the relationship of the atomic numbers for thorium and uranium is identical to that for uranium and plutonium; the relationships of the absorption coefficients, absorption edges, X-ray emission spectra, and fluorescence yields of one pair are therefore similar to these relationships for the members of the other pair. After most of the experimentation is performed with ThO_2-UO_2 (avoiding the hazards associated with plutonium), part of the data will be verified in experiments with UO_2-PuO_2.

1. Instrumental Considerations

The effect of resolution, count rates, and counting statistics of the collimator slit width in the X-ray fluorescence instrumentation has been studied.

a, Comparison of Collimators

There are nine identified processes in a flat-crystal spectrograph fluorescence apparatus where a loss of intensity can occur due to instrument effects; a major loss of fluorescence intensity is attributable to the fraction lost in collimation.[5]

A series of experiments was performed[6] with a Norelco spectrometer with different collimators. Ratemeter scans were obtained with a sample of 20% UO_2-80% ThO_2 for various combinations of collimators[7] having a slit

---

[4] H. P. Wickmann, M. DeCarolis, A. Mongon, and H. Eschrich, "Studies on the Determination of Uranium by X-ray Fluorescence in View of Its Application to Continuous On-Stream Analysis," NP-16417 (EIR-123) (1966).

[5] H. A. Liebhafsky, "X-ray Absorption and Emission in Analytical Chemistry," John Wiley & Sons, New York, 1960, p. 27.

[6] Experimental work performed by R. Schablaske, Analytical Section, Chemical Engineering Division, Argonne National Laboratory.

[7] The Norelco X-ray spectrum analyzer utilizes a collimater between the sample and the crystal and another collimator between the crystal and the detector.

widths of 5, 20, and 125 mils. The goal was to increase the precision within a fixed assay time by increasing the counting rate of each fluorescence peak. It was also desired to avoid a decrease in precision associated with a significant decrease in resolution or an excessive increase in background.

The data presented in Table 1 show that by using a 20-mil slit width for both collimators, the counting rates for thorium and uranium were each increased tenfold. A threefold increase in precision (far right column, Table 1) to 2.6% was obtained despite an increase in background. The half-width of both the thorium and uranium peaks increased, but not sufficiently to prevent resolution (except for the uranium peak for the case of a 125-mil slit width). Figure 1 illustrates that adequate separation of peaks was obtained with both collimators at a 20-mil spacing. The 20-mil collimator slit width will be used for subsequent experiments. The desired precision of $\pm 0.5\%$ was not achieved because these data were obtained with a ratemeter and represented low total counts.

An increase in the count rate for uranium to 7×10^3 cps was observed in recent experiments in which the X-ray tube was operated at 59 kV and 41 mA. At this count rate, a precision of $\pm 0.5\%$ at the 95% confidence level should be obtainable in a counting time of about 0.5 min. If the thorium peak and background counts are performed sequentially, as required on our Norelco instrument, the estimated total counting time for each pellet would be about 1 min.

These experiments have demonstrated that our existing counting equipment is not capable of handling the high count rate for the thorium peak. New Norelco counting equipment being installed for this program is expected to have a counting rate capability of 100,000 cps.

2. Materials Effects

The greatest loss of fluorescence intensity in X-ray fluorescence spectrometry is a result of re-emitted X-rays being only a small fraction of the X-rays striking the sample. Two kinds of variables affect the fraction re-emitted--absorption and enhancement. Absorption includes the effects of scattering from the surface, voids, and crystallites, as well as absorption in terms of the mass absorption coefficients of other elements present. Enhancement or secondary fluorescence occurs when the characteristic radiation from one element has enough energy to excite the characteristic radiation of one or more other elements in the sample. This occurs in uranium-plutonium oxides because PuLα excites ULα. In thorium-uranium oxides, ULα excites ThLα.

Experiments must be done to demonstrate whether variations in powder properties allow attainment of the necessary precision and accuracy. Normally, quantitative analysis by a fluorescence technique requires a set of standards covering the range of variables of interest, such as composition (element concentration and matrix content), density, crystallite size, and absorption coefficients. Criss and Birks[8] have formulated methods (utilizing

---

[8] J. W. Criss and L. S. Birks, Anal. Chem. 40, 1080 (1968).

Table 1

Comparison of Line Intensities at Several Collimator Slit Widths

80% ThO_2-20% UO_2 Powder
X-ray tube with tungsten target
Power: 45 kVP, 11 mA
3/8-in. dia mask
LiF diffraction crystal

Collimator Slit Width (mils)		Th 2θ Angle = 27.46°				U 2θ Angle = 26.13°					
Exit	Detector	Half Width (degree)	Gross (cps)	Bkgd. (cps)	Net (cps)	Half Width (degree)	Gross (cps)	Bkgd. (cps)	Net (cps)	Ratio	σ^b(%)
5	5	0.33	1203	30	1173	0.34	232	30	202	1	8.0
5	20	0.48	2080	61	2019	0.60	384	61	323	1.7	6.5
20	5	0.61	6157	160	5997	0.62	1126	173	953	5	3.8
125	5	0.75	8576	358	8218	c	1869	384	1485	7	3.9
20	20	0.78	12480	410	12070	0.91	2547	448	2099	10	2.6

[a] Ratio = uranium net count rate/net count rate with 5-mil slit width in both collimators.

[b] Relative standard deviation based on counting statistics limitation for uranium.

[c] Not measurable because of lack of resolution.

Figure 1

X-Ray Fluorescence Spectrogram, 80% ThO_2-20% UO_2 Powder

X-Ray Tube with Tungsten Target

Power: 45 kVp, 11 mA
Slit Width of Collimators: Exit 0.020 in.
Detector 0.020 in.
Full Scale: 12800 c/sec

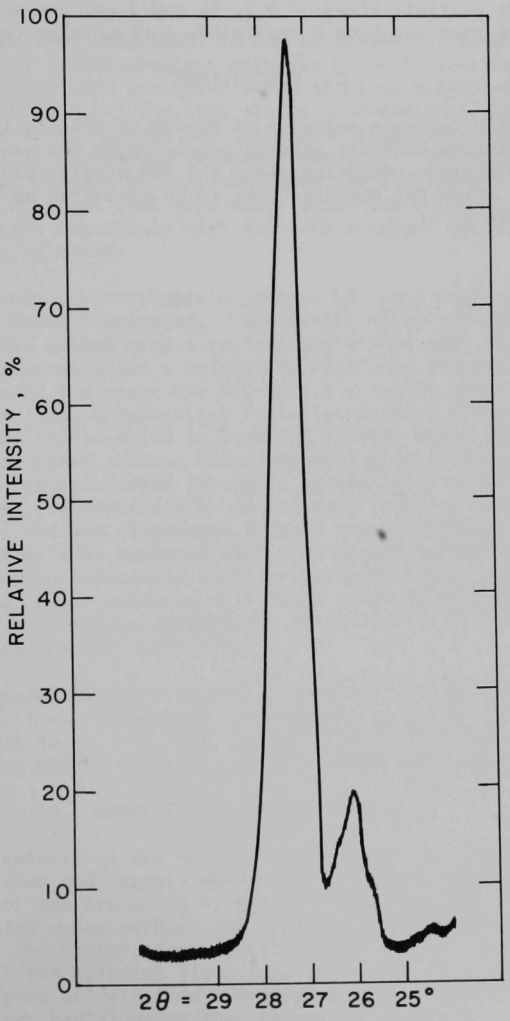

modern computers) whereby X-ray fluorescence can be calculated from fundamental parameters. Computer calculations should greatly decrease the number of standards necessary by allowing some prediction of signal losses due to material effects. Nevertheless, experimental work will be required to verify the effect of certain variables on fluorescence intensity for samples having varied plutonium content. These variables are particle size, particle density, bulk density, and O/M ratio.

Results of an exploratory experiment on three samples of coarse-grained (average particle sizes of 0.2, 1, and 2 mm) arc-melted UO_2 suggest that crystallite size may have a negligible influence on counting rate.

C. CONCLUSIONS

X-ray fluorescence analysis of powder or pellets to determine uranium and plutonium contents appears promising on the basis of experiments with ThO_2-UO_2 mixtures. Counting rates for the uranium peak have been large enough to allow the analysis time to be estimated as being one minute per sample.

IV. ADAPTATION OF CENTRIFUGAL CONTACTORS IN LMFBR FUEL PROCESSING

(G. Bernstein, J. Lenc, N. Quattropani)

Centrifugal contactors with 10-in. dia rotor bowls and with settling zones ~13 in. long are presently being used at Savannah River (SR) to process production reactor fuels. A Purex solvent extraction process is employed to separate uranium and plutonium from fission products at throughputs of 40-60 gpm.

A program has been undertaken at ANL to extend the Savannah River contactor design to a configuration suitable for efficient handling of plutonium in the plutonium isolation steps of Purex solvent-extraction processing of LMFBR fuels. The high plutonium content of the feed and product solutions in the second and third plutonium cycles requires the use of contactors of critically favorable geometry. The basic objective of the development program is to investigate the performance characteristics of centrifugal contactors that have small diameters for criticality control yet maintain relatively high capacity by means of increased bowl length and operating speed.

A stainless steel centrifugal contactor has been designed for testing and is currently being fabricated. This design is an adaptation of the Savannah River unit design with a restriction placed upon the stator diameter in order to maintain a critically favorable diameter. The stator ID is 4 3/4 in., and the rotor has a 4-in. ID x 0.1-in. wall. This contactor has a mixing paddle and a separating rotor (centrifuge bowl) mounted on a common shaft. The paddle spins in a mixing chamber below the hollow rotor. Organic and aqueous feed streams enter the bottom of the mixing chamber. The mixed phases are discharged through a nozzle into the interior of the rotor. The phases are separated by centrifugal force as they flow up through the rotor and are discharged through separate ports into collecting rings. This unit will be operated with a two-phase system at speeds up to ~3600 rpm to determine hydraulic capacity and efficiency. Natural uranium solutions containing no plutonium or fission products will be used. Background information regarding development of this contactor appears in the preceding quarterly report, ANL-7735.

While the stainless steel contactor is being fabricated, a different contactor design, i.e., an annular centrifugal contactor, is being tested using plastic test units. In this design, a simplified rotor is used and there is no mixing paddle or mixing chamber below the rotor.

A. ANNULAR CENTRIFUGAL CONTACTOR

The basic features of the annular centrifugal contactor are shown in Fig. 1. The aqueous and organic phases enter through inlet lines on the wall of the stator and are mixed by skin friction as they flow downward through the annular space between the spinning rotor and the stator. At the bottom of the stator, four radial baffles convert some of the kinetic energy of the spinning fluid into pressure. The mixed phases flow through a rotor orifice into the rotor and are quickly brought up to rotor speed by four radial vanes that extend to the top of the rotor. The

Figure 1

Annular Centrifugal Contactor

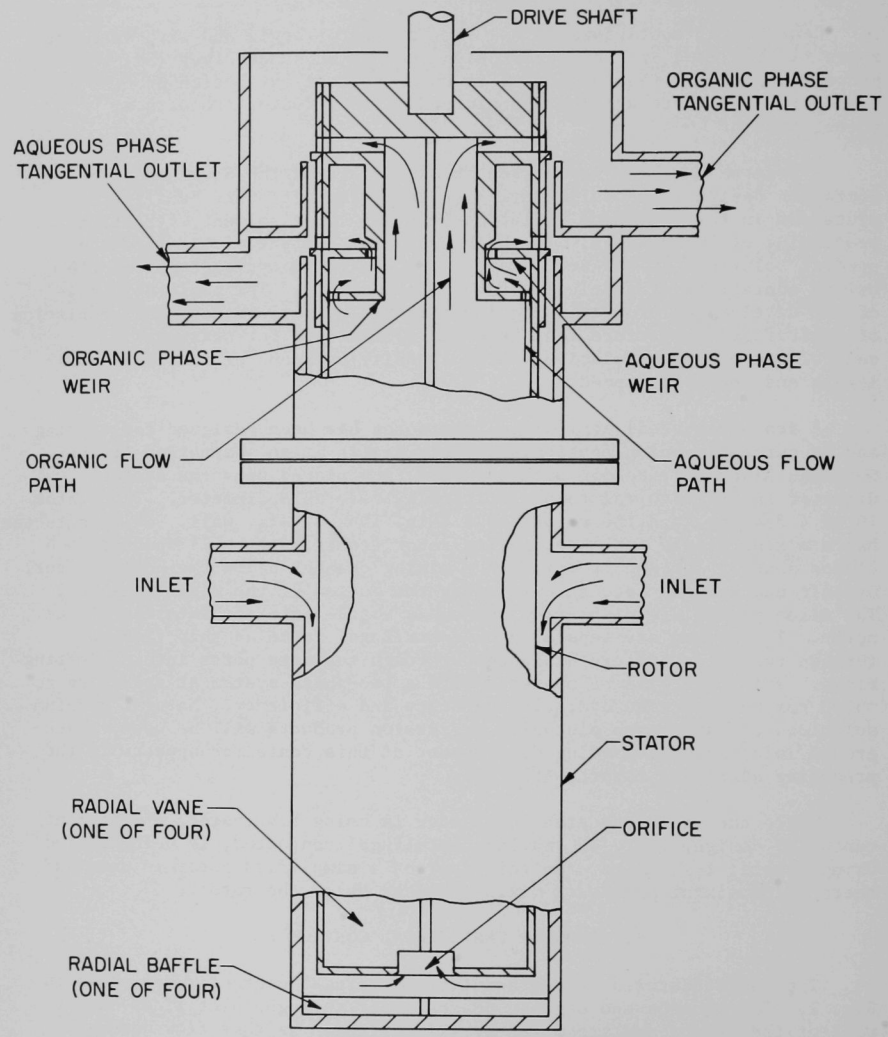

two phases are separated under centrifugal force and are discharged through ports into separate collecting rings.

A plastic contactor of annular design is being tested. A simple stationary weir is used to control the flow of the separated phases. A more versatile air-controlled weir similar to that used in the SR units can also be incorporated in the annular type of contactor. Two stators, one with a 4 1/2-in. ID and the other with a 5-in. ID, allowed operation with a 1/4- or 1/2-in. wide annulus.

The principal advantages sought in the annular design (as compared with the Savannah River design) are simpler fabrication, lighter weight (which may result in a higher critical speed for a rotor with a high length-to-diameter ratio), and possibly hydrodynamic support for the spinning rotor by fluid in the annular space.

An improved mixing pattern in the annular mixer might also be anticipated. Both phases enter near the top of the annular region and are mixed as they flow downward toward the rotor orifice. Consequently, it is extremely unlikely that any portion of an inlet stream will bypass the mixing region and be inadequately mixed.

1. Throughput Tests

Preliminary tests were performed with the plastic annular contactor to measure the rate of water throughput through the rotor. These tests were performed on a dynamometer test stand where the maximum rotor speed was ∿1800 rpm, depending upon the type of test being run.

Single-phase tests with water were made at various rotor speeds, with three sizes of rotor orifices, and with two different sizes of stators. With a 1/4-in. wide annular space essentially full of water (a 9 3/4-in. depth), throughputs were 9.9, 9.6, and 6.6 gpm with rotor orifices of 1 1/2-, 1-, and 3/4-in. dia, respectively. These throughput rates were essentially constant over a rotor speed range of ∿1000 to ∿1650 rpm.

As expected, at lower throughput rates (controlled by the input rate of water to the contactor), the level of water in the annulus was lower than at the greater throughput rates.

Increasing the annular gap to 1/2 in. by the use of a 5-in. ID stator and the 4-in. OD rotor resulted in the throughput increasing slightly to 11.7 gpm with a 1 1/8-in. orifice in the rotor. With the same stator, throughput decreased slightly when shallow vertical baffles were installed on the stator wall at either the top or bottom of the stator.

The stability of the throughput over the rotor speed range tested suggests that, with the particular rotor used in the test, throughput was limited by flow through the orifice rather than by pumping capacity of the rotor (which would be expected to increase at higher rotor speeds). It is also apparent that throughput is dependent on the height of liquid in the annulus. The annular type contactor may have a lower capacity than a unit of the same size based on the SR design because the mixing chamber

in the SR unit functions as a small centrifugal pump to provide additional head for injecting fluid into the rotor.

It was observed in these tests that the rotor spun more smoothly when the annulus was filled to a high level than to a low level, indicating that the fluid in the annulus provided some dynamic support.

2. Mixing Power Input and Mixing Intensity

To obtain an indication of the intensity of mixing that can be developed in the annular space, mixing power tests were performed. In these tests, a dynamometer test stand was used in which the torque delivered by the drive motor is balanced by an applied tangential weight. Power input is calculated from the speed and torque.

In these tests, the rotor orifice was sealed to make the system non-flowing and prevent power being consumed in pumping fluid through the rotor. Since the level of liquid in the annulus differs at different flow rates, power input was measured at two levels of water in the annulus.

With the 4 1/2-in. ID stator installed in the contactor, tests were made over a range of rotor speeds with ~9-in. water depth in the annulus. Power input ranged from 0.01 hp at 910 rpm to 0.07 hp at 1870 rpm. In other tests with a water level of ~5 in. in the annulus, the power input was about 70% of these values over the same range of rotor speeds.

A test was performed with a 5-in. depth of 50-50 mixture of water and refined kerosene in the annulus to measure the power consumed in mixing an emulsion. Power input values were about 50% higher than for water alone.

In these tests, the increase in power input with speed was somewhat less than a third-order rise. This departure may be attributed to vortexing of liquid in the annulus, which reduces the area of contact between the rotor and the liquid at high speeds. The radial baffles at the bottom of the stator may also have distorted the power input relationship that would exist between a smooth spinning rotor and a smooth stator.

In tests with the 5-in. ID stator installed in the contactor, essentially the same power input values were found as with the 4 1/2-in. ID stator. At a given flow rate, residence time in the annulus with the larger stator would be about twice the residence time with the smaller. Therefore, the intensity of mixing a discrete volume of liquid in the larger annulus would be lower than in the smaller annulus, and the mixing time would be longer. The lower mixing intensity might decrease the degree of emulsification of a two-phase system and the difficulty of subsequent separation.

On the basis of the power input measurements made in the above tests, an indication of the effectiveness of mixing in the plastic contactor can be found. Treybal[1] has related mixing power input to throughput in a

[1] R. E. Treybal, "Liquid Extraction," McGraw-Hill, 2nd ed., 1963, p. 427.

contacting vessel and has derived a relationship for predicting the effectiveness of contacting for achieving efficient mass transfer. The formula predicts good contacting when

$$P/Q \gtrsim 200$$

where P = power input, ft-lb/sec

Q = flow rate, ft^3/sec

For a total throughput of mixed phases of 10 gpm (0.022 ft^3/sec) and with mixing at 2000 rpm at a power input of about 0.1 hp (55 ft-lb/sec), then

$$P/Q = \frac{55}{0.022} = 2500.$$

This result suggests that intensive phase contacting is developed within the annular space of the ANL contactor and that effective mass transfer should occur in an operating two-phase system.

B. FUTURE WORK

When installation of the plastic contactor in the contactor test facility (now underway) is completed, throughput and phase-separating capacity will be measured during operation at rotor speeds up to 3600 rpm with a two-phase system. The stainless steel contactor, which can be operated as either an annular or SR design, will be installed in the test facility when fabrication is completed to permit comparison of its performance under the two modes of operation.

X

B